JPL D-11400, Revision G

Earth Observing System


Multi-angle
Imaging
Spectro-
Radiometer

# Level 2 Aerosol Retrieval Algorithm Theoretical Basis

David J. Diner[1]
Wedad A. Abdou[1]
Thomas P. Ackerman[2]
Kathleen Crean[1]
Howard R. Gordon[3]
Ralph A. Kahn[1]
John V. Martonchik[1]
Stuart McMuldroch[1]
Susan R. Paradise[1]
Bernard Pinty[4]
Michel M. Verstraete[4]
Menghua Wang[3]
Robert A. West[1]

[1]Jet Propulsion Laboratory, California Institute of Technology
[2]Pacific Northwest National Laboratory
[3]University of Miami
[4]Joint Research Centre


**Jet Propulsion Laboratory**
California Institute of Technology

March 10, 2008

JPL D-11400, Revision G

Multi-angle Imaging SpectroRadiometer (MISR)

# Level 2 Aerosol Retrieval Algorithm Theoretical Basis

Approval:

David J. Diner
MISR Principal Investigator

Approval signatures are on file with the MISR Project.
To determine the latest released version of this document, consult the MISR web site (http://www-misr.jpl.nasa.gov).

**Jet Propulsion Laboratory**
California Institute of Technology

# TABLE OF CONTENTS

# GLOSSARY OF ACRONYMS

**A**

ACP (Aerosol Climatology Product)

AGP (Ancillary Geographic Product)

APOP (Aerosol Physical and Optical Properties)

ARP (Ancillary Radiometric Product)

ARVI (Atmospherically-Resistant Vegetation Index)

ASAS (Advanced Solid-state Array Spectroradiometer)

ASL (Above Sea Level)

ASTER (Advanced Spaceborne Thermal Emission and Reflectance radiometer)

ATB (Algorithm Theoretical Basis)

AU (Astronomical Unit)

AVHRR (Advanced Very High Resolution Radiometer)

**B**

BRF (Bidirectional Reflectance Factor)

**C**

CCD (Charge-Coupled Device)

**D**

DAAC (Distributed Active Archive Center)

DAO (Data Assimilation Office)

DDV (Dense Dark Vegetation)

**E**

ECS (EOSDIS Core System)

EOF (Empirical Orthogonal Function)

EOS (Earth Observing System)

EOSDIS (Earth Observing System Data and Information System)

**F**

FOV (Field-of-View)

**G**

GDQI (Geometric Data Quality Indicator)

GEMI (Global Environmental Monitoring Index)

**H**

HC (High Confidence)

**I**

IAMAP (International Association for Meteorology and Atmospheric Physics)

IFOV (Instantaneous Field Of View)

**J**

JPL (Jet Propulsion Laboratory)

**L**

LC (Low Confidence)

**M**

MISR (Multi-angle Imaging SpectroRadiometer)

MODIS (Moderate Resolution Imaging Spectroradiometer)

**N**

NDVI (Normalized Difference Vegetation Index)

NOAA (National Oceanic and Atmospheric Administration)

**P**

ppmv (parts per million by volume)

**R**

RCCM (Radiometric Camera-by-camera Cloud Mask)

RDQI (Radiometric Data Quality Indicator)
RH (Relative Humidity)
RMS (Root-Mean-Square)
RT (Radiative Transfer)

**S**

SAGE (Stratospheric Aerosol and Gas Experiment)
SCF (Scientific Computing Facility)
SDCM (Stereoscopically Derived Cloud Mask)
SDP (Science Data Production)
SMART (Simulated MISR Ancillary Radiative Transfer)
SOM (Space Oblique Mercator)

**T**

TASC (Terrestrial Atmosphere and Surface Climatology)

**W**

WCP (World Climate Programme)
WGS (World Geodetic System)
WMO (World Meteorological Organization)

# INTRODUCTION

## 1.1 Purpose

This Algorithm Theoretical Basis (ATB) document describes the algorithms used to retrieve the aerosol parameters of the MISR Level 2 Aerosol/Surface Product. These parameters are summarized in Table 1. In particular, this document identifies sources of input data, both MISR and non-MISR, which are required for aerosol retrieval; provides the physical theory and mathematical background underlying the use of this information in the retrievals; includes implementation de tails; and describes assumptions and limitations of the adopted approach. It is used by the MISR Science Data System Team to establish requirements and functionality of the data processing software.

| Parameter name | Units | Horizontal Sampling (Coverage) | Comments |
|---|---|---|---|
| ***OptDepthPerMixture***: Aerosol optical depths per mixture | none | 17.6 km (Global) | • For each candidate aerosol compositional mixture used in the retrieval<br>• Reported at 558 nm |
| ***AerRetrSuccFlagPerMixture***: Compositional mixture identifiers | none | 17.6 km (Global) | • True for all candidate mixtures used in the retrieval<br>• Mixture information found in Aerosol Climatology Product |
| ***RegMeanSpectralOptDepth***, ***RegMedianSpectralOptDepth***, ***RegLowestResidSpectralOptDepth***: Regional estimates of aerosol optical depth | none | 17.6 km (Global) | • Determined from retrieval and computing mean, median, and lowest residual of successful model(s)<br>• Reported in all four spectral bands |
| ***RegLowestResidSpectralAngstromExponent***: Regional estimates of aerosol Angstrom exponent | none | 17.6 km (Global) | • Determined by calculating the Angstrom exponent from the regional lowest residual optical depths |
| ***RegBestEstimateSpectralOptDepth, RegBestEstimateAngstromExponent***: Best estimates of aerosol optical depth and Angstrom exponent | none | 17.6 km (Global) | • Determined from the regional mean optical depths, with missing optical depths filled in by averaging surrounding regions when sufficient neighboring data are available. Quality flag ***RegBestEstimateQA*** records where the filling in is done. |
| ***RegMeanSpectralSSA***, ***RegLowestResidSpectralSSA***: Regional estimates of aerosol single scattering albedo | none | 17.6 km (Global) | • Determined from retrieval and computing mean and lowest residual of successful model(s)<br>• Reported in all four spectral bands |
| ***RegMeanSpectralOptDepthFraction(1:3)***, ***RegLowestResidSpectralOptDepthFraction(1:3), RegLowestResidNumberFraction(1:3), RegLowestResidVolumeFraction(1:3)***: Regional | none | 17.6 km (Global) | • Determined from retrieval and computing mean and lowest residual of successful model(s)<br>• Reported in all four spectral bands<br>• Lowest residual number fraction reported |

| | | | |
|---|---|---|---|
| estimates of aerosol small, medium, and large particle optical depth fraction | | | • Lowest residual volume fraction reported |
| ***RegMeanSpectralOptDepthFraction(4:5)***, ***RegLowestResidSpectralOptDepthFraction(4:5), RegLowestResidNumberFraction(4:5), RegLowestResidVolumeFraction(4:5)***: Regional estimates of aerosol spherical and nonspherical particle optical depth fraction | none | 17.6 km (Global) | • Determined from retrieval and computing mean and lowest residual of successful model(s)<br>• Reported in all four spectral bands<br>• Lowest residual number fraction reported<br>• Lowest residual volume fraction reported |
| ***RegBestEstimateSpectralOptDepthFraction***, ***RegBestEstimateNumberFraction***, ***RegBestEstimateVolumeFraction***: Best estimates of aerosol particle properties | none | 17.6 km (Global) | • Determined from regional lowest residual estimates<br>• The "best estimate" (i.e. the model with the lowest combined residual) is only used if that model is also a successful model. |
| Retrieval quality indicators | varies | 17.6 km (Global) | • Retrieval applicability, algorithm type, retrieval residuals, parameter uncertainties, summary statistics, and other quality assessment indicators |
| Ancillary meteorological and atmospheric data | varies | 17.6 km (Global) | • Includes ozone optical depth, wind speed, and ambient pressure assumed in the retrieval, and source of data |

The MISR Aerosol/Surface Product is generated routinely during the EOS mission as new images are acquired. Certain information required to interpret the Aerosol/Surface Product, such as properties of the aerosol particles used to generate the compositional models used during the retrievals, and the relative abundances of the components in the mixtures, is incorporated in the Aerosol Climatology Product (ACP). These products are deliverable to the EOS user community through the Distributed Active Archive Center (DAAC), but are generated at the MISR Science Computing Facility (SCF), with the possibility of being updated during the mission. The contents and theoretical basis of the ACP parameters are provided in *[M-11]*.

## 1.2 SCOPE

This document covers the algorithm theoretical basis for the aerosol parameters of the Aerosol/Surface Product which are routinely retrieved at the DAAC. Specialized products or parameters are not discussed. Current development and prototyping efforts may result in modifications to parts of certain algorithms.

Chapter 1 describes the purpose and scope of the document. Chapter 2 provides a brief overview. The processing concept and algorithm description are presented in Chapter 3. Chapter 4 summarizes assumptions and limitations. References for publications cited in the text are given in Chapter 5.

## 1.3 MISR DOCUMENTS

Reference to MISR Project or reference documents is indicated by a number in italicized

square brackets as follows, e.g., *[M-1]*. The MISR web site (http://www-misr.jpl.nasa.gov) should be consulted to determine the latest released version of each of these documents.


*[M-1]* Experiment Overview, JPL D-13407.

*[M-2]* Level 1 Radiance Scaling and Conditioning Algorithm Theoretical Basis, JPL D-11507.

*[M-3]* Level 1 Georectification and Registration Algorithm Theoretical Basis, JPL D-11532.

*[M-4]* Level 1 Cloud Detection Algorithm Theoretical Basis, JPL D-13397.

*[M-5]* Level 1 In-flight Radiometric Calibration and Characterization Algorithm Theoretical Basis, JPL D-13398.

*[M-6]* Level 1 Ancillary Geographic Product Algorithm Theoretical Basis, JPL D-13400.

*[M-7]* Level 1 In-flight Geometric Calibration Algorithm Theoretical Basis, JPL D-13399.

*[M-8]* Level 2 Cloud Detection and Classification Algorithm Theoretical Basis, JPL D-11399.

*[M-9]* Level 2 Top-of-Atmosphere Albedo Algorithm Theoretical Basis, JPL D-13401.

*[M-10]* Level 2 Surface Retrieval Algorithm Theoretical Basis, JPL D-11401.

*[M-11]* Level 2 Ancillary Products and Datasets Algorithm Theoretical Basis, JPL D-13402.

*[M-12]* Science Data Validation Algorithm Theoretical Basis, JPL D-13403.

*[M-13]* In-flight Radiometric Calibration and Characterization Plan, JPL D-13315.

*[M-14]* In-flight Geometric Calibration Plan, JPL D-13228.

*[M-15]* Science Data Validation Plan, JPL D-12626.

*[M-16]* Science Data Processing Sizing Estimates, JPL D-12569.

*[M-17]* Science Data Quality Indicators, JPL D-13496.

## 1.4 REVISIONS

The original version of this document was dated February 23, 1994. Revision A was released December 1, 1994. Revision B was released August 15, 1996. Revision C was released December 3, 1997. Revision D was released December 2, 1999. Revision E was released April 10, 2001. Revision F was released October 6, 2006. This version is Revision G.

# 2. EXPERIMENT OVERVIEW

## 2.1 OBJECTIVES OF MISR AEROSOL RETRIEVALS

Aerosols are solid or liquid airborne particulates of various compositions, frequently found in stratified layers. Generally, they are defined as atmospheric particles with sizes between about 0.1 μm and 10 μm, though the sizes of condensation nuclei are typically about 0.01 μm. Under normal conditions, most of the atmospheric aerosol resides in the troposphere. Natural sources (e.g., dust storms, desert and soil erosion, biogenic emissions, forest and grassland fires, and sea spray) account for about 90% of this aerosol, with the rest resulting from anthropogenic activity (Williamson, 1972). The background tropospheric aerosol is temporally and spatially variable.

The overall objectives of the MISR aerosol retrievals are:

(1) To study, on a global basis, the magnitude and natural variability in space and time of sunlight absorption and scattering by aerosols in the Earth's atmosphere, particularly tropospheric aerosols, and to determine their effect on climate;

(2) To improve our knowledge of the sources, sinks, and global budgets of aerosols;

(3) To provide atmospheric correction inputs for surface imaging data acquired by MISR for the purpose of making better quantitative estimates of surface reflectance.

A scientific background on each of these objectives, a historical perspective on aerosol retrievals using remote sensing, the unique contributions of MISR, and a scientific rationale for the aerosol parameter contents of the MISR Aerosol/Surface Product are presented in *[M-1]*.

## 2.2 INSTRUMENT CHARACTERISTICS

The MISR instrument consists of nine pushbroom cameras. It is capable of global coverage every nine days, and flies in a 705-km descending polar orbit. The cameras are arranged with one camera pointing toward the nadir (designated An), one bank of four cameras pointing in the forward direction (designated Af, Bf, Cf, and Df in order of increasing off-nadir angle), and one bank of four cameras pointing in the aftward direction (using the same convention but designated Aa, Ba, Ca, and Da). Images are acquired with nominal view angles, relative to the surface reference ellipsoid, of 0°, 26.1°, 45.6°, 60.0°, and 70.5° for An, Af/Aa, Bf/Ba, Cf/Ca, and Df/Da, respectively. Each camera uses four Charge-Coupled Device (CCD) line arrays in a single focal plane. The line arrays consist of 1504 photoactive pixels plus 16 light-shielded pixels per array, each 21 μm by 18 μm. Each line array is filtered to provide one of four MISR spectral bands. The spectral band shapes are approximately gaussian and centered at 446, 558, 672, and 866 nm.

MISR contains 36 parallel chains corresponding to the four spectral bands in each of the nine cameras. The overlap swath width of the MISR imaging data (that is, the swath seen in common by all nine cameras) is 380 km, which provides global multi-angle coverage of the

entire Earth in 9 days at the equator, and 2 days near the poles. The crosstrack IFOV and spacing between centers of each pixel (i.e., the sample spacing) is 275 m for all of the off-nadir cameras, and 250 m for the nadir camera. Downtrack IFOVs depend on view angle, ranging from 214 m in the nadir to 707 m at the most oblique angle. Sample spacing in the downtrack direction is 275 m in all cam eras. The instrument is capable of buffering the data to provide 4 sample x 4 line, 2 sample x 2 line, or 1 sample x 4 line averages, in addition to the mode in which pixels are sent with no averaging. The averaging capability is individually selectable within each of the 36 channels, and there are several observational modes of the MISR instrument. The MISR Aerosol/Surface Product is generated from Global Mode data. Global Mode refers to continuous operation with no limitation on swath length. Global coverage in a particular spectral band of one camera is provided by operating the corresponding signal chain continuously in a selected resolution mode. Any choice of averaging modes among the nine cameras that is consistent with the instrument power and data rate allocation is suitable for Global Mode. Currently the instrument operates in the 4 x 4 averaging mode (1.1-km sampling) with selected channels operated in 1 x 1 mode. Use of higher resolution data benefits the aerosol retrievals by providing better cloud discrimination than would be achievable with the lower resolution data alone, and by providing other retrieval constraints.

Additional background on the instrument design is provided in *[M-1]*.

## 2.3 AEROSOL RETRIEVAL STRATEGY

In order to constrain the MISR aerosol retrievals, it is advantageous to make reasonable use of what is known about the types of aerosols that are found in the troposphere. In general, tropospheric aerosols fall into a small number of compositional categories, which include sea spray, sulfate/nitrate, mineral dust, biogenic particles (also referred to as carbonaceous particles), and urban soot (also referred to as black carbon particles). Approximate size ranges, and the proclivity of each particle type to adsorb water under increasing relative humidity are also known. Therefore, the MISR team has chosen an approach in which the physical and chemical (and therefore optical) properties of candidate aerosols are completely prescribed. The advantages of this approach, in contrast to a purely "generic" representation in terms of effective single scattering albedo, effective size distribution, and effective phase function, are that it potentially enables identification of aerosol sources and provides the means of extending aerosol properties retrieved at the MISR wavelengths to other spectral regions, which is useful for comparisons with other sensors and for model validation. To this end, a review of published aerosol climatologies was performed, including (d'Almeida et al., 1991), (Krekov, 1993), (Shettle and Fenn, 1979), (World Climate Programme WCP-112, 1984), and many others, and data from the Aerosol Robotic Network (AERONET) (Holben et al., 1998) and field campaigns analyzed. Aerosol attributes typical of natural conditions as described in these references (such as compositional and size classes) are adopted in the MISR retrievals. However, other attributes, such as aerosol amount and specific spatial and temporal distributions, are not assumed.

A summary of the MISR aerosol retrieval strategy is as follows: Based on the data contained in the ACP, forward radiative transfer calculations are pre-computed to provide various components of the atmospheric radiation field in the 36 MISR channels. These are

contained in the Simulated MISR Ancillary Radiative Transfer (SMART) Dataset and supplemented by calculations performed during the retrievals at the DAAC. During routine processing, these calculations are binned into models that are observationally distinguishable by MISR. Two retrieval pathways, one over land and one over water, are utilized. A summary of the retrieval strategies is shown in Figure 1, and additional background is provided below. Optical depth constraints, such as the maximum allowable optical depth, based on the darkest radiance observed in the scene, are calculated. For heterogeneous surface retrievals, these constraints include requiring mixture-optical depth combinations to be similar in their HDRF angular and spectral shapes. The pre-calculated results are used in conjunction with the MISR observations and the constraints above to determine those models that provide good fits to the data, and to retrieve aerosol optical depth.

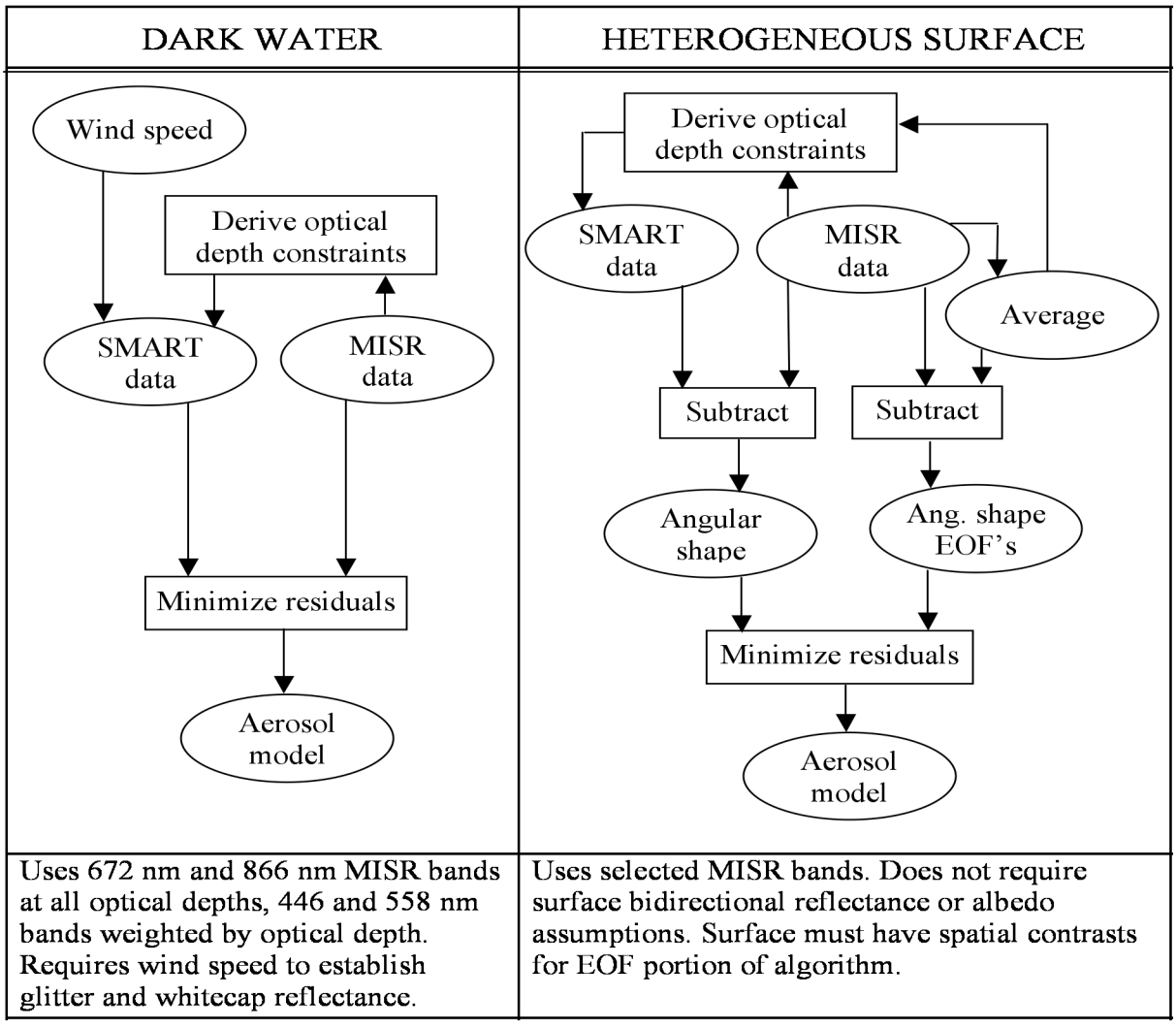


**Figure 1. MISR aerosol retrieval strategies**

### 2.3.1 Aerosol retrievals over dark water

Because of the reflectance uniformity of the large water bodies (e.g., the ocean), and the

fact that deep water bodies are essentially black at red and near-infrared wavelengths, considerable progress has been made in development of algorithms to retrieve aerosol properties over dark water. Under the assumption of an aerosol model (i.e., specification of particle size distribution, particle shape, and complex refractive index), it is possible using radiative transfer (RT) theory to derive a one-to-one relationship between observed radiance and aerosol optical depth. Such modeling has been applied to the retrieval of aerosol concentration from Landsat (Fraser, 1976), (Griggs, 1975) and NOAA AVHRR (Griggs, 1983), (Long and Stowe, 1993), (Rao et al., 1989), (Stowe et al., 1992), (Stowe et al., 1997). Substantial improvements in the retrieval of aerosol over ocean and other dark water bodies are possible with MISR. Multi-angle radiances, which are governed strongly by the shape of the aerosol scattering phase functions, provide additional information with which to refine the aerosol model used in the retrieval of optical depth.

### 2.3.2 Aerosol retrievals over land

The retrieval of aerosol optical depth over land from space is complicated by the brightness and heterogeneity of the land surface. The simplest means of determining the atmospheric contribution to the satellite signal is to make an assumption about the surface reflectivity or albedo. A method based on imaging over Dense Dark Vegetation (DDV) has been investigated (Kaufman and Sendra, 1988) and forms the basis of the MODIS aerosol retrieval over land (King et al., 1992). However, since dense vegetation is found only over a portion of the land surface, MISR multi-angle imaging enables the use other methods (Diner and Martonchik, 1985b), (Diner et al., 1994), (Martonchik and Diner, 1992), (Martonchik and Conel, 1994), (Martonchik, 1977). The basic heterogeneous land algorithm differs from the dark water retrieval method in that it does not use the observed radiances directly, but instead uses the presence of spatial contrasts to derive an Empirical Orthogonal Function (EOF) representation of the angular variation of the scene reflectance at the top-of-atmosphere, which is then used to estimate the scene path radiance (the radiance field reflected from the atmosphere without inter acting with the surface). This is used in turn to determine the best-fitting aerosol models. This revision of the ATB adds an extension to this algorithm, in which the spectral and angular shapes of the reflectance function are required to be invariant. HDRF angular and spectral shape similarity constraints have been used successfully by investigators using data from the Along-Track Scanning Radiometer-2 (ATSR-2); e.g., (Mackay et al., 1998) and (North et al., 1999).

# 3. ALGORITHM DESCRIPTION

## 3.1 PROCESSING OUTLINE

### 3.1.1 Processing flow

Processing flow concepts are shown diagrammatically throughout the document. The convention for the various elements displayed in these diagrams is shown in Figure 2.

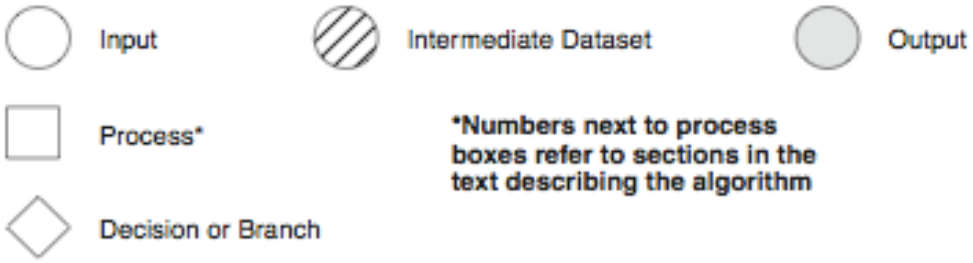


**Figure 2. Conventions used in processing flow diagrams**

The aerosol retrieval process is assisted by establishment of three ancillary datasets that are generated at the MISR SCF and then delivered to the DAAC. Further details are provided in *[M-11]*. These datasets are:

(1) The Terrestrial Atmosphere and Surface Climatology (TASC) Dataset, which provides climatological meteorological and ozone fields.
(2) The Aerosol Climatology Product (ACP), which consists of two component parts: an aerosol physical and optical properties file containing microphysical and scattering characteristics of a set of aerosol types upon which the retrievals are based; and an aerosol mixture file, which specifies the mixtures of pure aerosol types which comprise candidate models to be used during the retrievals and in formation about the mixtures required during the retrievals.
(3) The Simulated MISR Ancillary Radiative Transfer (SMART) Dataset, which contains components of the radiation fields used to generate the model top-of-atmosphere equivalent reflectances to which the MISR observations are compared during the retrievals and is generated by performing radiative transfer calculations on stratified atmospheric models containing the aerosols found in the ACP. The calculations contained in the SMART Dataset include two surface boundary condition cases: (1) oceans or large dark water bodies, and (2) spectrally black surface, which is used in the retrievals over land.

The remaining elements of the retrieval occur during routine processing at the DAAC. The MISR aerosol retrieval approach depends upon whether the viewed region contains dark water or land. The output of the aerosol retrieval process is then used to generate the surface parameters which are also part of the Aerosol/Surface Product. A retrieval flag indicates which path was used for each set of measurements.

Figure 3 outlines the concept for the "Stage 1" DAAC processing in which the data within each 17.6-km region upon which the aerosol retrieval is potentially to be performed are screened using regional filters, averaged to the appropriate spatial resolutions required for the retrievals, normalized to an Earth-Sun distance of 1 AU, converted to equivalent reflectances, corrected for spectral out-of-band leakage, corrected for ozone absorption, and then screened using subregional filters. All subregions which are unusable according to any of these criteria are eliminated. Processing of a region proceeds only if a sufficient number of subregions and camera views survive these tests. Ancillary meteorological and atmospheric parameters required for the retrievals are also calculated in Stage 1.

Figure 4 is a schematic representation of the conceptual "Stage 2" retrieval processing path to be followed at the DAAC. In Stage 2, the processing path is determined and the aerosol retrieval algorithm to be used is identified according to the following hierarchy: (1) The minimum equivalent reflectances that survived Stage 1 processing are identified for the purpose of putting an upper bound on aerosol optical depth for non-cloudy atmospheres; (2) If sufficient numbers of clear subregions are present, and land is also present, the heterogeneous land algorithm pathway is selected; (3) The dark water algorithm is selected if the region is identified as open ocean or the interior of a large inland water body and sufficient numbers of clear subregions are present.

Figure 5 is a schematic representation of the conceptual "Stage 3" retrieval processing path to be followed at the DAAC. In Stage 3, the actual retrievals are performed, according to the algorithm type and pre-determined calculations provided by Stage 2.

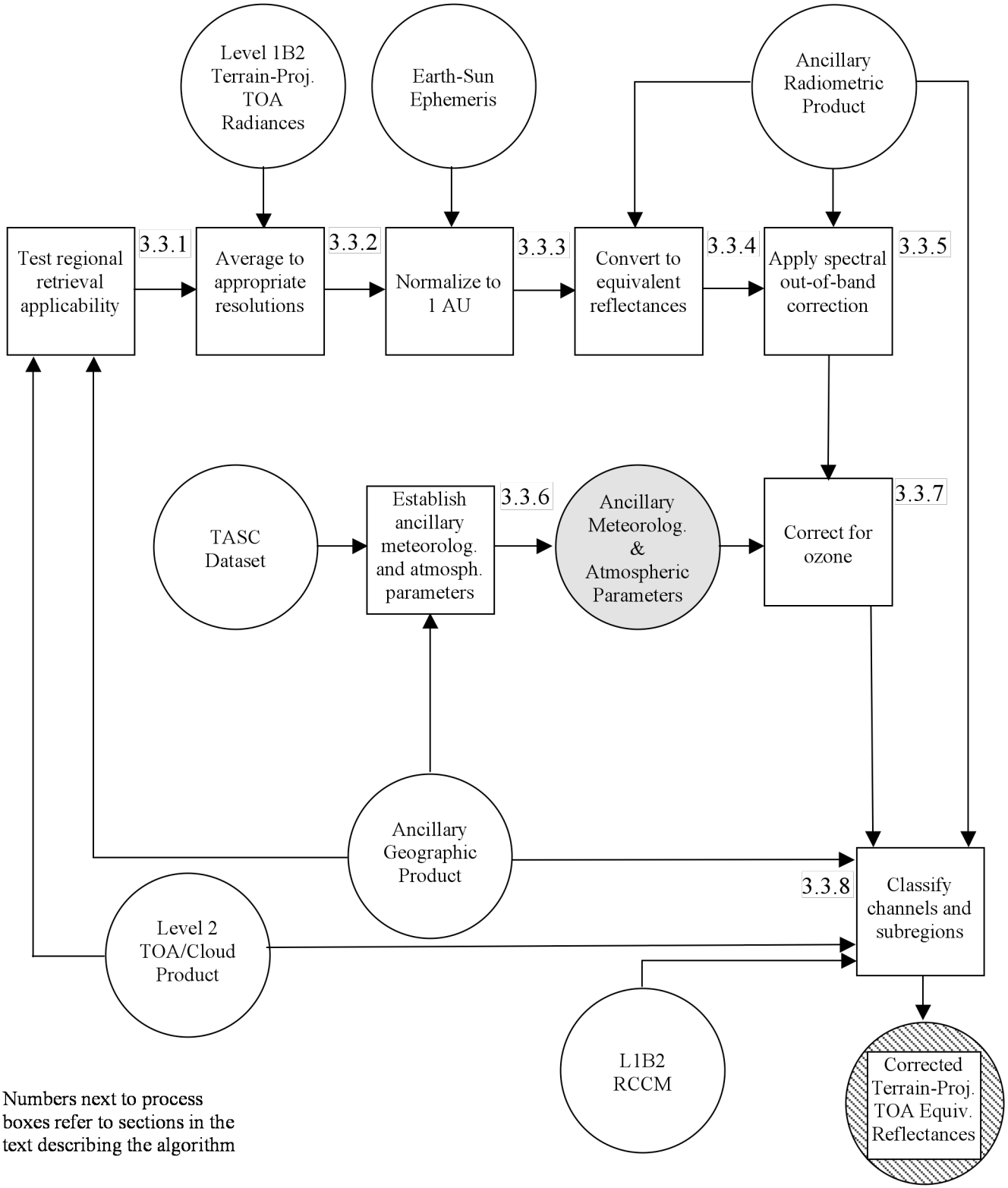


**Figure 3. Stage 1 retrieval processing concept**

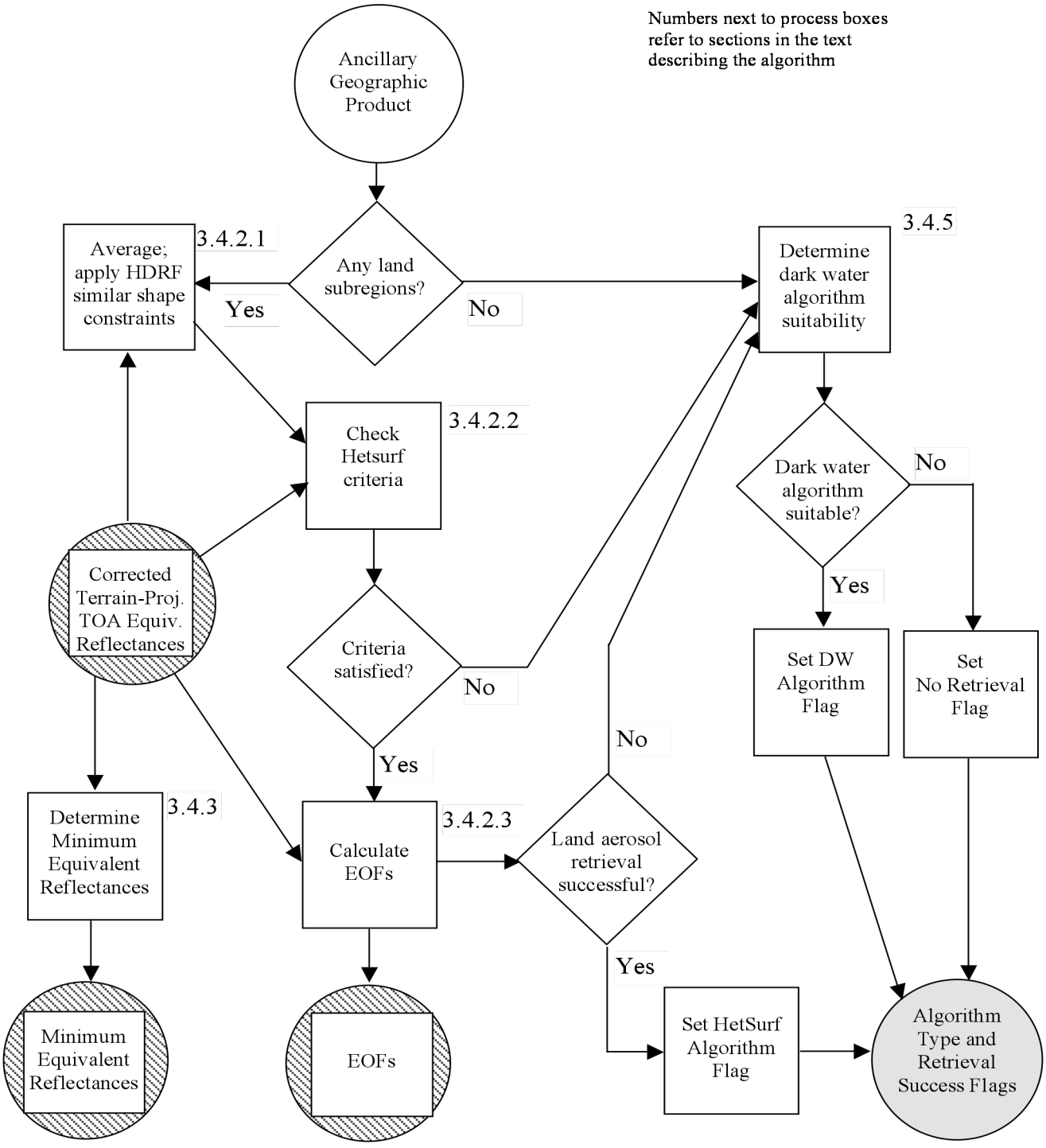


**Figure 4. Stage 2 retrieval processing concept**

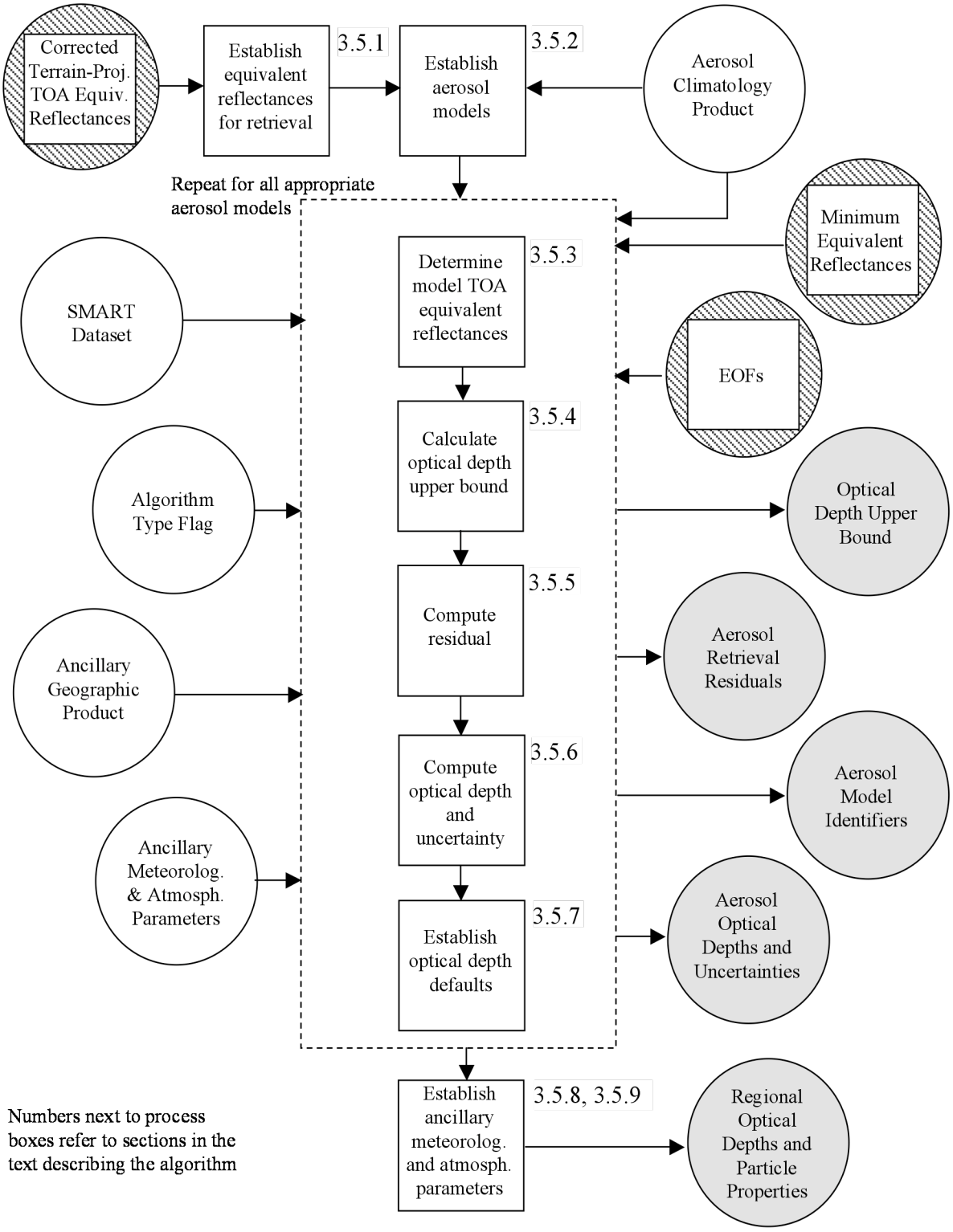


**Figure 5. Stage 3 retrieval processing concept**

### 3.1.2 Data staging and management

Aerosol retrievals are performed on 17.6-km regions, and for those regions containing land a surface retrieval is performed before the entire process shifts to the next region. In order to make the process efficient from a data staging standpoint, and to allow establishment of default optical depths over land, the manner in which the regions are stepped through is important.

A domain is defined to be a 70.4 km x 70.4 km area, that is, a 4 x 4 array of regions. Because the SMART Dataset is large, minimal re-staging of data is desirable. Parameters within SMART depend on view and illumination geometry. Therefore, regional geometric parameters are averaged over each domain, and SMART parameters corresponding to the domain-averaged geometry are used. Thus, all regions within a given domain are processed before moving on to the next domain and its associated set of regions.

Additionally, in order to maximize land surface retrieval coverage, default aerosol optical depths (and an associated aerosol model) are established when the land aerosol retrieval process fails to find a suitable model in a particular region. The method for setting these defaults is discussed in §3.5.7. Within each MISR 563.2 km x 140.8 km data block, there are 8 domains cross-track and 2 along-track, as shown in Figure 6. Regions within a domain are processed row by row.

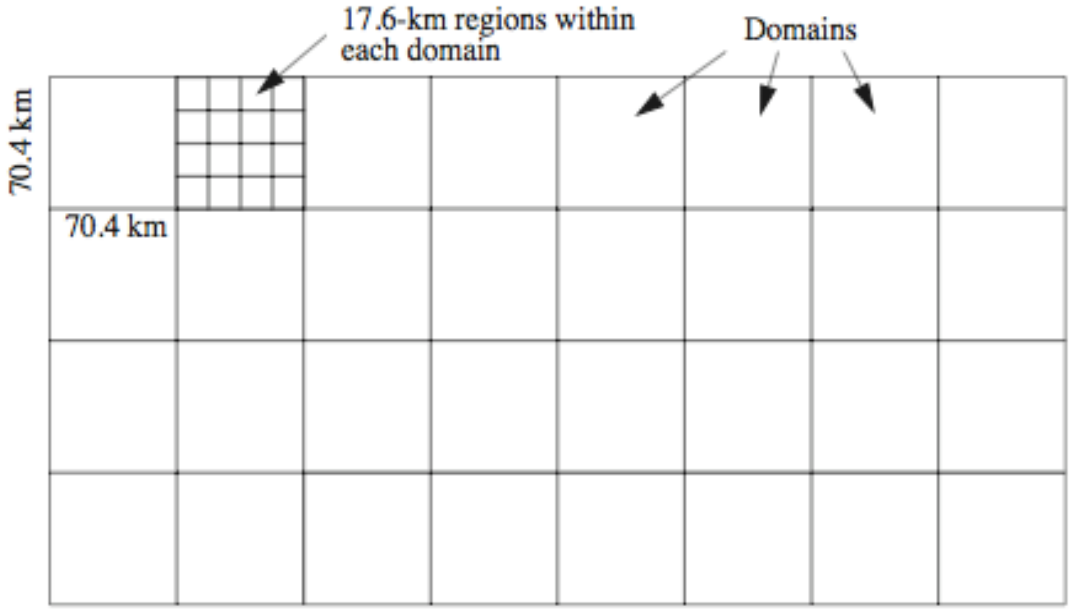


**Figure 6. Definition of regions and domains**

## 3.2 ALGORITHM INPUT

### 3.2.1 MISR data

Required inputs for the aerosol retrieval to be obtained from other parts of the MISR data system are summarized in Table 2 (see also Figures 3 - 5). Further information on each of the

inputs is provided below.

**Table 2: Aerosol/Surface Product inputs (MISR data) used for aerosol retrievals**

| Input data | Source of data | Reference |
|---|---|---|
| Terrain-projected TOA radiances | Level 1B2 Geo-rectified Radiance Product | *[M-3]* |
| Ellipsoid-projected TOA radiances | Level 1B2 Geo-rectified Radiance Product | *[M-3]* |
| Data Quality Indicators and Data Flags | Level 1B2 Geo-rectified Radiance Product | *[M-3]* |
| Ellipsoid-referenced geometric parameters | Level 1B2 Geo-rectified Radiance Product | *[M-3]* |
| Radiometric Camera-by-camera Cloud Mask (RCCM) | Level 2 RCCM Product | *[M-4]* |
| Stereoscopically Derived Cloud Mask (SDCM) | Level 2 TOA/Cloud Product | *[M-8]* |
| Angular Signature Cloud Mask (ASCM) | Level 2 TOA/Cloud Product | *[M-8]* |
| Land/water flags | Ancillary Geographic Product | *[M-6]* |
| Regional elevation data | Ancillary Geographic Product | *[M-6]* |
| Spectral out-of-band correction matrix | Ancillary Radiometric Product | *[M-5]* |
| Band-weighted exo-atmospheric solar irradiances | Ancillary Radiometric Product | *[M-5]* |
| Standardized solar-weighted band center wavelengths | Ancillary Radiometric Product | *[M-5]* |
| Pure aerosol optical properties | Aerosol Climatology Product | *[M-11]* |
| Aerosol mixture model specifications | Aerosol Climatology Product | *[M-11]* |
| Model TOA equivalent reflectances and radiative transfer parameters | SMART Dataset | *[M-11]* |

#### 3.2.1.1 Terrain-projected TOA radiances

The terrain-projected TOA radiance parameter is derived at Level 1B2 and consists of geolocated, registered, and calibrated radiances in all 36 channels of the instrument projected onto the surface terrain. A resampling process is required in order to implement this projection, and the effects of surface topography are taken into account. Terrain-projected radiances have not had any atmospheric correction applied and include both surface and atmospheric contributions to the signal. The data are resampled onto a Space Oblique Mercator grid. Note that the input from Level 1B2 consists of 16-bit integer words. Conversion of these integers to floating point values corresponding to radiances in the appropriate units (W $m^{-2}$ $sr^{-1}$ $\mu m^{-1}$) is accomplished by applying a multiplicative scale factor obtained from the Ancillary Radiometric Product (ARP).

#### 3.2.1.2 Ellipsoid-projected TOA radiances

Over oceans, the surface is assumed to correspond to the WGS84 ellipsoid. For this purpose, terrain-projected and ellipsoid-projected radiances are equivalent. To avoid duplication, these are stored in only one of the projected radiance parameter sets (the ellipsoid projection) generated during Level 1B2 processing. Thus, to access radiances over ocean, this parameter set must be ingested. Again, the data are encoded as 16-bit integers, which must be converted to radiances by the appropriate scaling, as discussed above.

#### 3.2.1.3 Data Quality Indicators and Data Flags

A Radiometric Data Quality Indicator (RDQI) is associated with each projected radiance provided by Level 1B2. This indicator provides a representation of the radiometric quality of the input radiances used to generate values reported in the Geo-rectified Radiance Product. Because of the data resampling required at Level 1B2, each projected radiance represents a bilinear interpolation of four surrounding radiances obtained from the MISR images. The radiances in the imagery are coded with a quality indicator specifying the reliability level of the radiometry on a pixel-by-pixel basis. From these, a scaled value is produced at Level 1B2. The RDQIs take on values of 0 - 3, as follows:

RDQI = 0: Radiometric accuracy meets all specifications

RDQI = 1: Radiometric accuracy is sufficient for certain applications but some specifications are violated (see *[M-2]* and *[M-3]*)

RDQI = 2: Radiance value is available but of insufficient accuracy to be used in Level 2 retrievals

RDQI = 3: Radiance value is unavailable.

Thus, higher quality data are associated with smaller values of RDQI.

In addition to the RDQIs, radiances reported in Level 1B2 are encoded to provide Data Flag information, for example, to indicate that a particular point on the Space Oblique Mercator (SOM) grid is topographically obscured from view by a particular camera.

Finally, MISR data have an associated Geometric Data Quality Indicator (GDQI). The GDQI provides a measure of how much image matching was used to insure high-quality image registration, relative to a pure reliance on spacecraft-supplied navigation.

#### 3.2.1.4 Ellipsoid-referenced geometric parameters

These are calculated at Level 1B2, and provide view zenith and azimuth angles as well as solar zenith and azimuth angles. They are also archived in the aerosol product as **SolZenAng**, V**iewZenAng**, **RelViewCamAziAng**, **ScatterAng**, and **GlitterAng**.

#### 3.2.1.5 Radiometric Camera-by-camera Cloud Mask (RCCM)

This is obtained from the MISR Level 1B2 Geo-rectified Radiance Product. It is used in combination with the Stereoscopically Derived Cloud Mask (SDCM) and Angular Signature Cloud Mask (ASCM) from the TOA/Cloud Product. The RCCM contains a mask to eliminate regions contaminated by sun glitter, derived on the basis that a particular view direction may be within a certain cone angle of the direction corresponding to specular reflection.

#### 3.2.1.6 Stereoscopically Derived Cloud Mask (SDCM)

The confidence levels associated with the retrieval of stereoscopic heights within the TOA/Cloud Product are used to generate a Stereoscopically Derived Cloud Mask. The algorithm for generating the SDCM within the TOA/Cloud retrievals incorporates the RCCM.

#### 3.2.1.6.a Angular Signature Cloud Mask (ASCM)

This is obtained from the MISR Level 2 TOA/Cloud Product. It is computed using the Band-Differenced Angular Signature technique.

#### 3.2.1.7 Cloud Shadow Mask

*This section is deleted. Cloud Shadow Masks are not computed by the Level 2 TOA/Cloud Product [M-8] as originally planned. Other techniques such as the band smoothness and angular correlation tests are being used to eliminate contaminated areas.*

#### 3.2.1.8 Topographic Shadow Mask

*This section is deleted. Topographic Shadow Masks are not computed by the Level 2 TOA/Cloud Product [M-8] as originally planned. Other techniques such as the band smoothness and angular correlation tests are being used to eliminate contaminated areas.*

#### 3.2.1.9 Regional cloud fraction

*This section is deleted. The Regional cloud fraction computed by the Level 2 TOA/Cloud Product [M-8] is not used by the Aerosol/Surface product as originally planned.*

#### 3.2.1.10 Land/water flags

These are obtained on 1.1-km centers from the Ancillary Geographic Product (AGP). This product is generated at the MISR SCF and stored at the DAAC. The land/water flag includes an indicator of water regions where application of the dark water aerosol retrieval algorithm is appropriate.

#### 3.2.1.11 Regional elevation data

These inputs consist of the mean surface elevation and standard deviation of surface elevation over 17.6-km regions, relative to the WGS84 reference ellipsoid. These data are

obtained from the AGP.

#### 3.2.1.12 Spectral out-of-band correction matrix

As described in §3.3.5, a spectral out-of-band correction is applied to MISR data to compensate for larger than desired energy outside the nominal in-band region of the spectral filters. This correction requires the use of a 4 x 4 matrix. The elements of this matrix are stored in the Ancillary Radiometric Product (ARP). This product is updated routinely at the MISR SCF and stored at the DAAC.

#### 3.2.1.13 Instrument measurement uncertainties and signal-to-noise ratios

*This section is deleted. Instrument measurement uncertainties and signal-to-noise ratios are no longer used by the Aerosol/Surface product.*

#### 3.2.1.14 Band-weighted exo-atmospheric solar irradiances

These are used to convert top-of-atmosphere radiances to equivalent reflectances. They are obtained from the ARP. There are several types of band-weighted exo-atmospheric solar irradiances, $E_0$, contained in the ARP, distinguished by how the spectrally-varying irradiances $E_{0\lambda}$ are weighted by the spectral response of the MISR cameras. During Level 1 processing of MISR data, a correction to the observed radiances is made to account for variations in the in-band spectral response from pixel-to-pixel and camera-to-camera. As a result, the conversion of radiances to equivalent reflectances required for aerosol retrievals make use of the parameters designated $E_{0,b}^{std}$ in the ARP (*[M-2]*, *[M-5]*) where the superscript *std* indicates weighting by a standardized spectral response over the total spectral range for which the cameras have measurable sensitivity, and the subscript *b* indicates that a value of this parameter is provided for each of the 4 instrument spectral bands.

#### 3.2.1.15 Standardized solar-weighted band center wavelengths

These parameters, denoted $\lambda_{m,solar,b}^{std,in-band}$ are the central wavelengths determined from a moments analysis, for each band, of the standardized in-band spectral response curve weighted by the exo-atmospheric solar irradiance spectrum. They are used as the band center wavelengths for the purpose of calculating Rayleigh scattering optical depth.

#### 3.2.1.16 Component aerosol optical properties

The aerosol prescriptions which form the basis of the MISR retrievals are stored in the Aerosol Climatology Product (ACP). One portion of this product contains physical properties (e.g., size distribution, index of refraction, and density), based upon current knowledge, and effective optical properties calculated using Mie theory for spherical particles, and ellipsoid approximations/geometric optics for non-spherical cases (Mishchenko et al., 1997). Each of these aerosols is considered “pure”, that is, of a single chemical composition and unimodal size

distribution. All aerosol particles are assumed to be spherical, except for mineral dust, which is modeled as grains.

The contents of the ACP and the theoretical basis behind its generation are described in *[M-11]*.

#### 3.2.1.17 Aerosol mixture model specifications

During routine aerosol retrievals at the DAAC, it is necessary to establish the mixtures of pure aerosols included in the ACP that will be compared to the MISR observations. For each region of the globe, an additional portion of the ACP defines those mixtures, for each of the retrieval path ways that may occur (i.e., dark water or heterogeneous surface), providing the component pure aerosol model identifiers, and the relative abundances of each component, defined in terms of fraction of total optical depth. In addition, this part of the ACP contains information required during the retrievals, such as optical depth spectral scaling factors and single-scattering albedos of the aerosol mixtures. The "clim-likely" part of the ACP, which assigns a likelihood value to each of the selected aerosol models, based on reasonable climatological expectations, has been de-scoped and is not included in the ACP. Details are provided in *[M-11]*.

#### 3.2.1.18 Model TOA equivalent reflectances and radiative transfer parameters

Using the optical properties of the aerosol models in the ACP, forward radiative transfer calculations are performed at the MISR SCF to calculate components of the top-of-atmosphere equivalent reflectance field, other top- and bottom-of-atmosphere radiometric parameters, and diffuse and total atmospheric transmittance. These are calculated for a variety of view and illumination geometries, corresponding to the range of values relevant to the MISR experiment. The results, for discrete values of total aerosol optical depth, and surface type, comprise the Simulated MISR Ancillary Radiative Transfer (SMART) Dataset.

We assume a multiple-layer, horizontally homogeneous atmosphere plus dark water surface model in generating the SMART Dataset. The Rayleigh scattering part of the atmosphere is assumed to be present in all the layers. For a given aerosol model, consisting of either tropospheric aerosol, stratospheric aerosol, or cirrus cloud, the altitude limits and scale height of the aerosol layer are specified. Atmospheric water vapor is modeled as being confined to the lowest layers. All layers are not simultaneously populated. A purely absorbing layer consisting of ozone is assumed to overlie all of the scattering layers, but is not included in the forward calculations; rather, a correction is made during the retrieval process (see §3.3.7).

For the aerosol retrievals over heterogeneous land surfaces, the radiation fields from the SMART Dataset are those corresponding to a black surface, and the effects of surface reflectance are accounted for during the actual retrievals. Over dark water, the pre-calculated radiation fields in the SMART Dataset provide an additional component assuming a surface model that accounts for Fresnel reflection and the effects of wind speed on sun glint and whitecaps.

Top-of-atmosphere equivalent reflectances, which form the basis for the MISR aerosol retrievals, are calculated using the doubling/adding method of solving the radiative transfer equation for plane-parallel geometry. These calculations are performed for the pure aerosol types contained in the ACP over a range of optical depths. The minor water vapor absorption affecting the MISR band 4 radiances is included in the forward calculations. In general, the radiance $L$ leaving the top of the atmosphere can be written as

$$L_{x,y}(-\mu,\mu_0,\phi-\phi_0) = L^{atm}(-\mu,\mu_0,\phi-\phi_0) + \\ +\exp(-\tau/\mu)\cdot\frac{1}{\pi}\int_0^1\int_0^{2\pi} R_{x,y}^{surf}(-\mu,\mu',\phi-\phi')L_{x,y}^{inc}(\mu',\mu_0,\phi'-\phi_0)\mu' d\mu' d\phi' + \\ +\frac{1}{\pi}\int_0^1\int_0^{2\pi}\int_0^1\int_0^{2\pi} T_{x,y}(-\mu,-\mu'',\phi-\phi'')\otimes R_{x,y}^{surf}(-\mu'',\mu',\phi''-\phi')L_{x,y}^{inc}(\mu',\mu_0,\phi'-\phi_0)\mu' d\mu'' d\phi'' d\mu' d\phi' \tag{1}$$

where x, y are the image spatial coordinates in a Cartesian coordinate system in which +z points toward the center of the Earth and is normal to the surface ellipsoid (not the local topographically-defined surface orientation), +x points toward the north pole, $\theta$ and $\theta_0$ are the view and Sun angles with respect to the +z axis, $\mu = |\cos\theta|$, $\mu_0 = |\cos\theta_0|$, $\phi_0$ is the azimuthal angle of the solar illumination vector, and $\phi$ is the azimuthal angle of a vector pointing toward the MISR instrument, also in the ellipsoid reference system. These definitions lead to the convention of using $-\mu$ and $\mu$ for upwelling and downwelling radiation respectively. The properties of the atmosphere are assumed to be horizontally homogeneous. On the right-hand-side of Eq. (1), $L^{atm}$ is the radiance field scattered by the atmosphere to space without interacting with the surface (i.e., the path radiance), $\tau$ is the optical depth of the total atmosphere, $L_{x,y}^{inc}$ is the direct and diffuse downward radiance field incident on the surface, $T$ is the upward diffuse transmittance, and $R_{x,y}^{surf}$ is the spatially variable surface bidirectional reflectance factor (BRF). The BRF of a surface target is defined as the bidirectional reflectance distribution function of the target ratioed to the bidirectional reflectance distribution function from a non-absorbing Lambertian surface (Nicodemus et al., 1977).

In the general three-dimensional solution to the radiative transfer problem with a horizontally uniform atmosphere over a spatially varying and flat surface, the transmittance $T_{x,y}$ can be thought of as a point-spread function and with the convolution operation $\otimes$ describes the blurring effect of the atmosphere on the surface reflectance $R_{x,y}^{surf}$ (Diner and Martonchik, 1985a). When the image spatial resolution is comparable to the atmospheric scattering scale height (defined by the vertical distribution of the aerosols and/or Rayleigh scattering molecules), Eq. (1) reduces to the standard one-dimensional radiative transfer regime, and $T$ is effectively a delta function in the spatial coordinates. In this case, Eq. (1) simplifies to:

$$L_{x,y}(-\mu,\mu_0,\phi-\phi_0) = L^{atm}(-\mu,\mu_0,\phi-\phi_0) +$$
$$+\exp(-\tau/\mu)\cdot\frac{1}{\pi}\int_0^1\int_0^{2\pi} R_{x,y}^{surf}(-\mu,\mu',\phi-\phi')L_{x,y}^{inc}(\mu',\mu_0,\phi'-\phi_0)\mu' d\mu' d\phi' +$$
$$+\frac{1}{\pi}\int_0^1\int_0^{2\pi}\int_0^1\int_0^{2\pi} T(-\mu,-\mu'',\phi-\phi'')R_{x,y}^{surf}(-\mu'',\mu',\phi''-\phi')L_{x,y}^{inc}(\mu',\mu_0,\phi'-\phi_0)\mu' d\mu'' d\phi'' d\mu' d\phi' \quad (2)$$

As described in §2.2, MISR data is acquired in various averaging modes. The 3-D radiative transfer regime is appropriate for the high-resolution channels (1 x 1 or 1 x 4) and the 1-D regime is appropriate for 4 x 4-averaged samples. A further simplification of Eq. (2) occurs over surfaces which are uniform in reflectance. For such cases, Eq. (2) is simplified by eliminating the *x, y* subscripts from the equation. Finally, in the case where the surface is black, only the path radiance term survives.

Since polarization of scattered light can affect the radiances measured by MISR, the effects of polarization are incorporated by correcting radiances in our scalar calculations by subtracting the contribution due to the Rayleigh scattering, including its interaction with the surface and then adding back this contribution as calculated with a vector code. The interaction of the polarized Rayleigh scattering from the atmosphere and the polarizing Fresnel reflection from the dark water surface is important for radiance calculations, and our correction takes this into account.

The ACP contains the optical properties of pure particles upon which the MISR retrievals are based, and the SMART Dataset contains radiometric quantities for these pure aerosols. During routine retrievals at the DAAC, mixtures of these aerosols are compared to the MISR observations. Mixing ratios are specified on a quantized grid. Sensitivity studies have been performed to determine which mixtures are distinguishable by the MISR instrument under the illumination and viewing conditions of the EOS orbit. Models observationally indistinguishable to within the measurement uncertainties of MISR are binned together, thus limiting the number of distinct combinations. The results dictate the various mixtures that are used in the retrieval process, yielding a substantial improvement over previous satellite-based retrievals of tropospheric aerosols. Modified linear mixing rules were used to generate the required radiometric properties of these mixtures. The relevant equations are provided in §3.5.3. The modified linear mixing equations described there require splitting the path radiance component of the TOA equivalent reflectance field into its single- and multiple-scattered components.

Additional details on SMART Dataset contents and generation are provided in *[M-11]*.

### 3.2.2 Non-MISR data

Required inputs for the aerosol retrieval to be obtained from non-MISR sources are summarized in Table 3. TASC data are specified for every month and year of the mission for the snow/ice

flag and surface wind speed due to the sensitivity of the retrievals to these parameters, and are specified for every month and replicated over year for other parameters. Further information on each of the inputs is provided below.

**Table 3: Aerosol/Surface Product inputs (non-MISR data) used for aerosol retrievals**

| Input data | Source of data |
|---|---|
| Earth-Sun ephemeris | SDP Toolkit |
| Column ozone abundance | Climatological values in the TASC Dataset |
| Meteorological variables (column precipitable water, surface pressure, surface temperature, temperature profile, geopotential height profile, near-surface wind speed) | Climatological values in the TASC Dataset |

#### 3.2.2.1 Earth-Sun ephemeris

This is used to obtain the Earth-Sun distance, such that observed radiances can be normalized to the standard distance of 1 AU. The source is the Science Data Production (SDP) Toolkit, which is generated by the EOSDIS Core System (ECS) contractor.

#### 3.2.2.2 Stratospheric aerosol optical depth and size distribution parameters

*This section is deleted. Stratospheric aerosol optical depth is not used as originally planned.*

#### 3.2.2.3 Column ozone abundance

The sensitivity of the MISR instrument to ozone is great enough to warrant applying a correction. Climatological values are obtained from the TASC Dataset.

#### 3.2.2.4 Meteorological variables

The following meteorological variables are used in the MISR aerosol retrievals. They are obtained from the climatological values provided in the TASC Dataset (see *[M-11]*). The use of each parameter in the retrieval process is briefly described.

##### *3.2.2.4.1 Column precipitable water*

Column precipitable water is not used to constrain the aerosol retrievals. However, it is reported with the Aerosol/Surface product.

##### *3.2.2.4.2 Relative humidity*

*This section is deleted. Relative humidity is not used as originally planned.*

#### *3.2.2.4.3 Surface pressure*

The surface pressure is used to establish the amount of Rayleigh scattering to include in the models used during the retrievals.

#### *3.2.2.4.4 Surface temperature*

The surface temperature is used in the calculation of pressure at an arbitrary altitude above sea level. It is obtained from the TASC Dataset.

#### *3.2.2.4.5 Geopotential height profile*

*This section is deleted. Geopotential height profiles are not used as originally planned.*

#### *3.2.2.4.6 Near-surface atmospheric wind speed*

In conjunction with a model of the effect of wind on water surface roughness, this parameter is used in the calculation of the TOA radiance field over dark water and for the purpose of identifying portions of each camera's FOV that may be contaminated by glitter, and for determining the lower boundary condition for dark water aerosol retrievals.

Because of the sensitivity of the L2 retrievals to wind speeds, these values are provided for every month and year of the mission.

#### *3.2.2.4.7 Snow/Ice mask*

This snow/ice mask is used during cloud mask determination. Stricter cloud masking is used over snow and ice regions because of the increased likelihood in these regions for the cloud masks to misclassify them as clear.

Because of the sensitivity of the L2 retrievals to cloud masking, which is more difficult over snow and ice, these values are provided for every month and year of the mission.

## 3.3 THEORETICAL DESCRIPTION: STAGE 1 RETRIEVAL PROCESSING

Figure 3 shows those processes which occur at the DAAC involving processing of the data prior to actual aerosol retrievals (referred to as Stage 1). In the following sections, the physical basis of these processes is described, and a mathematical description of the algorithm which is used to implement each process is presented.

### 3.3.1 Test regional retrieval applicability

#### 3.3.1.1 Physics of the problem

Several tests are applied to determine the suitability of using each sample observed in each of the MISR instrument channels for aerosol retrieval. The purpose of this step is to determine whether a particular 17.6 km x 17.6 km region is suitable for performing an aerosol retrieval. The regional retrieval applicability is archived in the aerosol product as ***RegClassInd***.

#### 3.3.1.2 Mathematical description of the algorithm

##### *3.3.1.2.1 Regional solar zenith angle test*

A region is deemed unacceptable for aerosol retrieval if the cosine of the solar zenith angle, $\mu_0$, is < 0.2 (***mu0_thresh*** in the aerosol science configuration file). The reason for this limitation is that plane-parallel radiative transfer theory is assumed for the retrievals, and this assumption breaks down for very oblique illumination angles.

##### *3.3.1.2.2 Regional topographic complexity test*

A region is classified as topographically complex, and unsuitable for aerosol retrieval, if the standard deviation of the regional surface elevation exceeds 500 m (***region_topo_complex_thresh*** in the aerosol science configuration file).

##### *3.3.1.2.3 Regional cloudiness test*

*This section is deleted. The Regional Cloud Masks in the Level 2 TOA/Cloud Product [M-8] is not used as originally planned.*

##### *3.3.1.2.4 Sufficient data test*

There are other reasons why a region may be determined to be unsuitable for aerosol retrieval. For example, application of the subregion-by-subregion and channel-by-channel tests (see §3.3.8) may eliminate so much data that when an attempt is made to apply a particular retrieval algorithm, there is an insufficient number of surviving subregions or channels. Another example is the heterogeneous land algorithm, which may determine that insufficient contrast was present. As opposed to the regional topographic complexity or regional cloudiness tests, these evaluations cannot be made until further processing has been accomplished.

### 3.3.2 Average subregion radiances

#### 3.3.2.1 Physics of the problem

Radiances provided by the MISR Level 1B2 Geo-rectified Radiance Product are in the same averaging mode in each channel as the data were acquired on orbit. For certain channels, these data need to be averaged to coarser resolution in order to apply the aerosol retrieval

algorithm (e.g., red band data acquired at 275-m sampling need to be averaged 4 lines x 4 samples in order to generate a 1.1-km input).

#### 3.3.2.2 Mathematical description of the algorithm

Averaging over all applicable samples is used as required to generate samples with the appropriate resolution for each algorithm. Thus, the output average radiance is given by:

$$L_{av} = \frac{\sum_{i,j} w(i,j)L(i,j)}{\sum_{i,j} w(i,j)} \tag{3}$$

where *L(i, j)* is the radiance for the $(i,j)^{th}$ sample, and the corresponding weight, *w*(i, j), is equal to 1 if the RDQI for the sample is $\leq RDQI_1$; otherwise *w*(i, j) = 0. We set $RDQI_1 = 1$ (***rdqi1*** in the aerosol science configuration file).

An RDQI value, $RDQI_{av}$, is also assigned to $L_{av}$. Its calculation takes into account the individual RDQIs as well as what proportion of the total number of 1x1 samples that make up the subregion, *N*, contain valid data. In generating a 1x4 (275 m cross-track x 1.1 km along-track) subregion from 1x1 data, for example, *N* = 4, and in generating a 4x4 (1.1 km cross-track x 1.1 km along-track) subregion, *N* = 16. We define

$$RDQI_{av} = nearest\ \ integer\left\{\frac{1}{N}\sum_{i,j} RDQI'(i,j)\right\} \tag{3a}$$

where $RDQI'(i,j) = RDQI(i,j)$ if $RDQI(i,j) \leq RDQI_1$; otherwise $RDQI'(i,j) = RDQI_2$. We set $RDQI_2 = 3$ (***rdqi2*** in the aerosol science configuration file).

In the event that $RDQI_{av} = 3$, $L_{av}$ is set to a flag value indicating "missing data". However, if $RDQI_{av} = 3$ and any of the *L(i, j)* is a flag value indicating "topographically obscured", $L_{av}$ is also set to the "topographically obscured" flag value.

### 3.3.3 Normalize to Earth-Sun distance of 1 AU

#### 3.3.3.1 Physics of the problem

The equivalent reflectances in the SMART Dataset are generated assuming a standard Earth-Sun distance of 1 AU. Because of the slight eccentricity of the Earth's orbit, MISR observations must be normalized to this distance before comparisons with the SMART Dataset can be made.

#### 3.3.3.2 Mathematical description of the algorithm

Letting $d$ be the Earth-Sun distance in AU, the normalization is simply made by multiplying the observed MISR radiances by $d^2$.

### 3.3.4 Convert to equivalent reflectances

#### 3.3.4.1 Physics of the problem

Top-of-atmosphere (TOA) radiometric information contained in the SMART Dataset and other ancillary sources are provided in the form of equivalent reflectances. In order to compare MISR measurements with the data from these sources, MISR radiances, $L$, must be converted to equivalent reflectances, ρ. Equivalent reflectance conceptually represents an arbitrary radiance level in terms of the particular value of reflectance of an exo-atmospheric Lambertian target, illuminated by the Sun at normal incidence, that would yield the same radiance at the sensor. For example, a perfectly reflecting Lambertian target illuminated by overhead Sun has a true reflectance and an equivalent reflectance of 1.0 at all view angles. If the same target were illuminated at a solar incidence angle of 60°, its true reflectance is still 1.0, but ρ = 0.5 (*cos* 60° × 1.0) at all view angles.

#### 3.3.4.2 Mathematical description of the algorithm

The conversion of radiance to equivalent reflectance is given by:

$$\rho = \pi L / E_{0,b}^{std} \tag{4}$$

where $L$ is the radiance within a given sample in band $b$ as provided by the Level 1B2 product, and $E_{0,b}^{std}$ is the band-weighted spectral exo-atmospheric solar irradiance for band $b$ as defined in §3.2.1.14.

### 3.3.5 Apply spectral out-of-band correction

#### 3.3.5.1 Physics of the problem

During pre-flight camera testing, it was discovered that the amount of out-of-band light is larger than called for in the spectral response specification by about a factor of three. For scenes of different spectral content than the Spectralon panels against which the MISR cameras are calibrated in flight, small radiometric errors result from the fact that the out-of-band integrated response is typically about 3% of the integrated in-band response. Thus, compensation for this phenomenon is desirable for the aerosol and surface retrievals, as the information contained in the ancillary datasets (ACP and SMART) assume that the radiation is essentially monochromatic at the MISR band-center wavelengths (an exception is the water vapor content of band 4 within the SMART Dataset, which is integrated over the instrument's spectral response). The correction approach requires co-registration of the four MISR bands in order to obtain an estimate of the scene spectrum. For these reasons, the correction is implemented at this stage of MISR systematic data processing.

#### 3.3.5.2 Mathematical description of the algorithm

The correction algorithm is applied to each subregion to be used in the MISR aerosol and/or surface retrievals. It requires a value of equivalent reflectance at each of the four MISR wavelengths. If less than the full complement of four bands is available, no correction is applied and the uncorrected values are used. The correction algorithm is implemented by applying the following equation:

$$\begin{bmatrix} \rho_1 \\ \rho_2 \\ \rho_3 \\ \rho_4 \end{bmatrix}_{corrected} = M \begin{bmatrix} \rho_1 \\ \rho_2 \\ \rho_3 \\ \rho_4 \end{bmatrix} \tag{5}$$

where the corrected equivalent reflectances are obtained from the uncorrected values by multiplying a column vector of the uncorrected values by $M$, a 4 x 4 correction matrix. Because this is a small correction, the matrix $M$ is dominated by its diagonal elements. The derivation underlying Eq. (5) assumes that the actual scene spectrum can be approximated, for the purposes of this correction, by a piecewise linear function constrained by the MISR observations and knowledge of the actual spectral response of the cameras (determined from pre-flight spectral calibration), the ideal spectral response, and solar irradiance spectrum (see *[M-5]*). The elements of $M$ are stored in the ARP.

If application of Eq. (5) results in any of the corrected equivalent reflectances becoming negative, this correction is skipped and the uncorrected equivalent reflectances are used.

### 3.3.6 Establish ancillary meteorological and atmospheric parameters

#### 3.3.6.1 Physics of the problem

The ancillary atmospheric parameters required for the aerosol retrievals are the ambient pressure, the column ozone abundance, and the near-surface wind speed. The mean terrain altitude of the 17.6-km region, $z$, is obtained from the AGP. The ambient pressure at this altitude, $P_z$, is derived by assuming hydrostatic equilibrium and a constant temperature lapse rate. This pressure is required for the determination of Rayleigh scattering optical depth and for establishing the pressure to which the inputs from the SMART Dataset are interpolated. Column ozone abundance does not include any correction for terrain altitude, as all terrain heights are beneath the bulk of the ozone. Near-surface wind speed is used only in the dark water retrievals. Column precipitable water is also ingested and reported with the product, although it is not currently used in the retrievals.

#### 3.3.6.2 Mathematical description of the algorithm

Pressure at height $z$, $P_Z$, is given by:

$$P_z = P_s \cdot F(z, z_0) \tag{6}$$

where $P_s$ is the surface pressure in hPa, $z_0$ is the mean altitude of the grid cell in the TASC Dataset, and $F(z,z_0)$ is a function to correct for the difference in the average altitude of the 17.6-km region ($z$) and the average altitude of the TASC grid cell ($z_0$), and is given by

$$F(z, z_0) = \exp\left[\frac{-c(z - z_0)}{T_s}\right] \quad \text{for } 0.99 \leq t \leq 1.01$$

$$F(z, z_0) = t^{\left[\frac{c(z - z_0)}{T_s(1-t)}\right]} \quad \text{otherwise} \tag{7}$$

where $t$ is the ratio of the atmospheric temperature at altitude $z$ to the surface air temperature, expressed in Kelvins, and is obtained by linearly interpolating the temperature profile to altitude $z$, $c$ is a constant equal to 34 K km$^{-1}$, and $T_s$ is the surface air temperature.

Near-surface wind is provided by the TASC Dataset as vector components $U$ and $V$ in m/sec. Scalar wind speed $W$ for dark water retrievals is calculated from

$$W = \sqrt{U^2 + V^2} \tag{7a}$$

### 3.3.7 Correct for ozone absorption

#### 3.3.7.1 Physics of the problem

Top-of-the-atmosphere (TOA) equivalent reflectances obtained by MISR include a small effect due to ozone absorption. The ratio of column extinction optical depth due to ozone, relative to that due to Rayleigh scattering, for each of the MISR bands, has been calculated according to:

$$R_i = \frac{\int \tau_{ozone}(\lambda) f_i(\lambda) d\lambda}{\int \tau_{Rayleigh}(\lambda) f_i(\lambda) d\lambda} \tag{8}$$

where $R_i$ is the ratio for filter $i$, $f_i$ is the filter response at wavelength λ, and $\tau_{ozone}$ and $\tau_{Rayleigh}$ are the wavelength-dependent ozone and Rayleigh optical depths. Climatological global averaged ozone values are around 300 Dobson units, and range from a high of 460 near the Arctic Circle in northern spring to 180 in the Antarctic ozone "hole" in southern spring (World Meteorological Organization, 1998). For 300, 400, and 450 Dobson unit ozone columns, in a 1000 mb atmosphere at 193 K, the results for the MISR bands are shown in Table 4.

**Table 4: Ozone optical depths relative to Rayleigh optical depths in the MISR spectral bands**

| Band | $R_i$ (300 Dobsons) | $R_i$ (400 Dobsons) | $R_i$ (450 Dobsons) | $\tau_{Rayleigh}$ |
|---|---|---|---|---|
| 1 | 0.00721 | 0.00961 | 0.0108 | 0.236 |
| 2 | 0.332 | 0.443 | 0.498 | 0.094 |
| 3 | 0.333 | 0.445 | 0.500 | 0.044 |
| 4 | 0.0738 | 0.0971 | 0.112 | 0.016 |

The final column in Table 4 gives the Rayleigh extinction optical depth at band center, for each MISR band. From this table, an upper bound on the ozone optical depth in MISR bands 2 and 3 is about 0.5 of the Rayleigh contribution, requiring correction. An accuracy of about 20 Dobson units in the column abundance is needed for these corrections, suggesting that climatology values are adequate for all but the most extreme ozone events. Upper bounds on the ozone extinction are 10% of the Rayleigh contribution in band 4, and 1% in band 1. For comparison, aerosol extinction optical depths of interest to the MISR experiment are about 0.05 or greater.

Since the majority of the ozone resides in the stratosphere, correction of the MISR equivalent reflectances for ozone absorption is accomplished by assuming that sunlight is directly attenuated only, by an amount depending on the ozone amount and the sun-camera geometry.

#### 3.3.7.2 Mathematical description of the algorithm

For the MISR aerosol retrieval, column abundance of ozone, provided by the TASC Dataset in Dobson units, is converted to ozone optical depth in each of the MISR channels, and used as input to the TOA equivalent reflectance correction.

*Equation deleted* (8a)

*Equation deleted* (8b)

*Equation deleted* (8c)

*Equation deleted* (8d)

The relationship between column ozone optical depth, $\tau_{ozone}$, and ozone abundance, $D_{ozone}$, is

$$\tau_{ozone}(\lambda) = c_{\lambda} D_{ozone} \tag{9}$$

where $c_\lambda$ is equal to 5.67 x $10^{-6}$, 1.04 x $10^{-4}$, 4.89 x $10^{-5}$, and 3.94 x $10^{-6}$, respectively, for bands 1

through 4.

The ozone correction is straightforward to implement, since ozone only absorbs light, and is written:

$$\left[\rho(-\mu,\mu_0,\phi-\phi_0)\right]_{ozone\_corrected} = \rho(-\mu,\mu_0,\phi-\phi_0)\cdot\exp\left[\tau_{ozone}\left(\frac{1}{\mu}+\frac{1}{\mu_0}\right)\right] \quad (10)$$

### 3.3.8 Classify channels and subregions

#### 3.3.8.1 Physics of the problem

In this step, aerosol retrieval applicability is tested on a subregional (1.1 km x 1.1 km), camera-by-camera, or channel-by-channel basis. The following tests are done in sequential fashion. If a particular subregion or channel is found to be unusable or contaminated according to a certain test, the remaining tests are not performed. A retrieval applicability mask, consisting of a 16 x 16 array corresponding to each of the subregions within a 17.6-km x 17.6-km region, is generated for each of the 36 channels of MISR, and contains a flag indicating either that retrieval is acceptable or the name of the test which resulted in an unusable or contaminated designation. The retrieval applicability mask is archived as ***RetrAppMask*** in the aerosol product.

#### 3.3.8.2 Mathematical description of the algorithm

##### *3.3.8.2.1 Missing data test*

Any subregion and channel for which there is an indication of missing data is flagged as unsuitable for aerosol retrieval.

##### *3.3.8.2.2 Topographic obscuration test*

Any subregion equivalent reflectance corresponding to an input radiance that has been encoded to indicate that the surface view is obscured by topography is considered unacceptable for aerosol retrieval in that camera.

##### *3.3.8.2.3 Glitter contamination test*

If a particular subregion is classified as anything other than Land in the AGP, and also exceeds the aerosol science configuration file parameter ***glitter_threshold*** (currently set to 40.0˚) at a particular view angle, all bands at that angle are deemed unsuitable for aerosol retrieval. For subregions classified as Land, the glitter test is not applied. Although there may be spatially unresolved water bodies within the subregion, snow or ice may be present, or there may have been recent rainfall giving rise to sun glint, the angle-to-angle smoothness test (see §3.3.8.2.9) is used to detect and filter out the affected subregions. This strategy preserves as much data as possible for utilization in the aerosol retrievals while ensuring that unsuitable data are screened.

#### *3.3.8.2.4 Topographic shadow test*

*This section is deleted. The topographic shadow test is not employed as originally planned.*

#### *3.3.8.2.5 Topographic complexity evaluation*

Subregions of topographic complexity are defined to be those for which the root-mean-square (RMS) elevation variation exceeds 250 m (***subr_complex_topo_thresh*** in the aerosol science configuration file), or for which the average slope exceeds 20° (***max_subr_avg_slope*** in the aerosol science configuration file), as determined from the AGP. In this event, all channels are unacceptable for aerosol retrieval.

#### *3.3.8.2.6 Cloud masking*

The RCCM, SDCM, and ASCM cloud masks are used together to determine whether a particular subregion is considered cloud contaminated. Mathematical details of the RCCM are provided in *[M-4]*, and details of the SDCM and ASCM are provided in *[M-8]*. If any camera is designated cloudy in a subregion, the subregion is not used in the aerosol retrieval. The cloudy cameras are labeled as such in the RetrAppMask field, and the other cameras are labeled "cloudy other camera".

##### *3.3.8.2.6.1 Land/water regions*

The logic shown in Figure 7 below is used in determining whether a given camera view of a subregion corresponds to a cloudy or clear scene in land and water regions. This logic is captured in the **cloud_mask_decision_matrix** in the aerosol science configuration file.

| | | **RCCM** | | | | |
|---|---|---|---|---|---|---|
| | | No Retrieval | CloudHC | CloudLC | ClearLC | ClearHC |
| **SDCM** | No Retrieval | Clear | Clear | Clear | Clear | Clear |
| | CloudHC | Clear | Cloud | Cloud | Clear | Clear |
| | CloudLC | Clear | Cloud | Cloud | Clear | Clear |
| | NearSurfaceLC | Clear | Clear | Clear | Clear | Clear |
| | NearSurfaceHC | Clear | Clear | Clear | Clear | Clear |

**Figure 7. Land/water cloud decision matrix**

##### *3.3.8.2.6.2 Snow/ice regions*

Scenes identified by the TASC as being snow/ice covered employ a more conservative

cloud logic, including the addition of the ASCM, because of the difficulty in distinguishing clouds from snow and ice. This strategy is afforded due to increased coverage at high latitudes. Figure 8 shows the logic used to determine whether a given camera view for a snow/ice scene is cloudy or clear.

| **ASCM= No Retrieval** | | **RCCM** | | | | |
|---|---|---|---|---|---|---|
| | | No Retrieval | CloudHC | CloudLC | ClearLC | ClearHC |
| **SDCM** | No Retrieval | Cloud | Cloud | Cloud | Clear | Clear |
| | CloudHC | Cloud | Cloud | Cloud | Cloud | Cloud |
| | CloudLC | Cloud | Cloud | Cloud | Cloud | Cloud |
| | NearSurfaceLC | Clear | Cloud | Cloud | Clear | Clear |
| | NearSurfaceHC | Clear | Cloud | Cloud | Clear | Clear |

| **ASCM= CloudHC** | | **RCCM** | | | | |
|---|---|---|---|---|---|---|
| | | No Retrieval | CloudHC | CloudLC | ClearLC | ClearHC |
| **SDCM** | No Retrieval | Cloud | Cloud | Cloud | Cloud | Cloud |
| | CloudHC | Cloud | Cloud | Cloud | Cloud | Cloud |
| | CloudLC | Cloud | Cloud | Cloud | Cloud | Cloud |
| | NearSurfaceLC | Cloud | Cloud | Cloud | Cloud | Cloud |
| | NearSurfaceHC | Cloud | Cloud | Cloud | Cloud | Cloud |

| **ASCM= CloudLC** | | **RCCM** | | | | |
|---|---|---|---|---|---|---|
| | | No Retrieval | CloudHC | CloudLC | ClearLC | ClearHC |
| **SDCM** | No Retrieval | Cloud | Cloud | Cloud | Cloud | Cloud |
| | CloudHC | Cloud | Cloud | Cloud | Cloud | Cloud |
| | CloudLC | Cloud | Cloud | Cloud | Cloud | Cloud |
| | NearSurfaceLC | Cloud | Cloud | Cloud | Cloud | Cloud |
| | NearSurfaceHC | Cloud | Cloud | Cloud | Cloud | Cloud |

| **ASCM= ClearLC** | | **RCCM** | | | | |
|---|---|---|---|---|---|---|
| | | No Retrieval | CloudHC | CloudLC | ClearLC | ClearHC |
| | No Retrieval | Clear | Cloud | Cloud | Clear | Clear |
| | CloudHC | Cloud | Cloud | Cloud | Cloud | Cloud |

| | | | | | | |
|---|---|---|---|---|---|---|
| **SDCM** | CloudLC | Cloud | Cloud | Cloud | Cloud | Cloud |
| | NearSurfaceLC | Clear | Cloud | Cloud | Clear | Clear |
| | NearSurfaceHC | Clear | Cloud | Cloud | Clear | Clear |
| **ASCM= ClearHC** | | **RCCM** | | | | |
| | | No Retrieval | CloudHC | CloudLC | ClearLC | ClearHC |
| **SDCM** | No Retrieval | Clear | Cloud | Cloud | Clear | Clear |
| | CloudHC | Cloud | Cloud | Cloud | Cloud | Cloud |
| | CloudLC | Cloud | Cloud | Cloud | Cloud | Cloud |
| | NearSurfaceLC | Clear | Cloud | Cloud | Clear | Clear |
| | NearSurfaceHC | Clear | Cloud | Cloud | Clear | Clear |

**Figure 8. Snow/ice cloud decision matrix**

#### *3.3.8.2.7 Cloud shadow masking*

*This section is deleted. A Cloud Shadow Mask is not be provided by the Level 2 TOA/Cloud Product [M-8] as originally planned, and is not used during processing.*

#### *3.3.8.2.8 Data quality evaluation*

Only subregions and channels for which the Radiometric Data Quality Indicator is ≤ a threshold RDQI value $RDQI_3$ are deemed acceptable for aerosol retrieval. $RDQI_3$ is presently set to 0 (***rdqi3*** in the aerosol science configuration file). Geometric Data Quality Indicators from Level 1B2 are reported as part of the Aerosol/Surface Product but are not used to reject regions for processing.

#### *3.3.8.2.9 Brightness test*

Large, bright clouds sometimes lack the texture necessary to be picked up by the Stereoscopically-Derived Cloud Mask. These regions are easily identified by their brightness. In this test, if the BRFs of all spectral bands for any camera exceed a threshold (***bright_thresh*** in the aerosol science configuration file), the subregion is eliminated for all cameras, with the camera triggering the brightness being labeled “too bright”, and the other cameras labeled “bright other camera” in the retrieval applicability mask. The threshold is currently set to 0.5 for land, 0.5 for water, and to 1.0 for snow/ice, effectively turning the test off over snow and ice subregions. Camera angles in glint are not included in this test. The brightness test does not over-ride subregions that were identified as “clear” by the RCCM.

#### *3.3.8.2.10 Angle-to-angle smoothness evaluation*

This is a test to insure that the equivalent reflectance field is "smooth" as a function of angle. Clouds, glitter, or other effects which have escaped detection using other methods may be amenable to detection using this test. It is applied to each spectral band separately, and to the forward + nadir camera set independently of the aftward + nadir camera set. Failure of the smoothness test for either set causes the subregion, in the spectral band being examined, to be eliminated from aerosol processing (but not from surface processing).

The presence of rainbows in the scattering phase function of an atmospheric aerosol can cause the angular variation of equivalent reflectance to not be smooth. Currently, "rainbow-influenced" cameras are simply flagged as such, and archived in the aerosol product in the CamRainbowFlag field.

The algorithm works as follows for each camera set (forward + nadir or aftward + nadir). For the available cameras in each set, we calculate the scattering angle, Ω, defined by

$$\cos\Omega = -\mu\mu_0 + (1-\mu^2)^{\frac{1}{2}}(1-\mu_0^2)^{\frac{1}{2}}\cos(\phi-\phi_0) \tag{11}$$

Any camera for which Ω is in the range $\Omega_1$ to $\Omega_2$ is then flagged as "rainbow-influenced"; if Ω is not in this range the camera is "rainbow-free". We set $\Omega_1$ = 110° (***min_rainbow_dw_omega*** in the aerosol science configuration file) and $\Omega_2$ = 160° (***max_rainbow_dw_omega***) if the AGP indicates that the subregion is suitable for dark water retrieval; we also set $\Omega_1$ = 110° (***min_rainbow_omega***) and $\Omega_2$ =160° (***max_rainbow_omega***) for non-dark-water retrievals. Although the rainbow-influenced cameras are flagged and reported in the product parameter ***CamRainbowFlag***, they are not eliminated from the smoothness test as originally planned.

We then count the number of available cameras in the set which have not been eliminated by previous tests. If this number is < 4, this test is skipped for that camera set.

If there are either 4 or 5 available cameras, the subregion equivalent reflectances are then fit to a polynomial with one less degrees of freedom than the number of cameras, that is, a quadratic polynomial in the case of 4 cameras and a cubic polynomial in the case of 5 cameras. Let $\rho_{poly,k}$ be the polynomial fit value of equivalent reflectance for camera *k*, and let $\rho_{MISR,k}$ be the corresponding measured value. Now calculate the parameter

$$\chi^2_{smooth} = \frac{1}{N_C}\cdot\sum_{k=1}^{N_C}\frac{(\rho_{MISR,k}-\rho_{poly,k})^2}{\sigma^2_{cam,k}} \tag{12}$$

where $N_c$ is the number of cameras in the set (i.e., 4 or 5) and $\sigma_{cam,k}$ is the relative camera-to-

camera radiometric uncertainty in $\rho_{MISR,k}$. The value of $\sigma_{cam,k}$ is estimated to be

$$\sigma_{cam,k} = 0.03\rho_{MISR,k} \tag{12a}$$

If a value of $\chi^2_{smooth}$ is obtained for either the forward + nadir or aftward + nadir set (or both), and if either of these values exceeds 4 (***chisq_smooth_thresh*** in the aerosol science configuration file), the subregion is considered unacceptable for aerosol retrieval.

#### *3.3.8.2.11 Angle-to-angle correlation evaluation*

The angle-to-angle correlation mask is designed to detect features which result in poor correlation of the equivalent reflectance spatial distribution from one view angle to another, e.g. a cloud within a subregion that may have been missed by the standard cloud masks. This algorithm is unique in that it makes use of the 4 x 4 arrays of 275-m red band equivalent reflectances in each 1.1-km subregion which has survived previous tests. Poor correlation results in subregions being eliminated from aerosol processing, but *not* from surface processing.

The first step is to generate a camera-averaged "template" 4 x 4 image from the 275-m red band data for subregions which have not been eliminated by previous tests. The equivalent reflectance of pixel *i, j* in the template image, $\rho_t(i,j)$, is calculated to be a data quality-weighted average of the equivalent reflectances of all cameras, where the RDQI corresponds to each 275-m sample. That is, we calculate:

$$\rho_t(i,j) = \frac{\sum_k w_k(i,j)\rho_k(i,j)}{\sum_k w_k(i,j)} \tag{13}$$

where the sum over *k* refers to the available cameras, $\rho_k(i,j)$ is the equivalent reflectance in pixel *i, j* for the $k^{th}$ camera, and $w_k(i,j)$ = 1 if the RDQI associated with $\rho_k(i,j)$ is ≤ $RDQI_4$; otherwise $w_k(i,j)$ = 0. If the denominator in Eq. (13) is zero, that is, all cameras have RDQI > $RDQI_4$ in a particular pixel, the value of $\rho_t(i,j)$ is undefined. This does not matter because in the following steps of the algorithm, pixels for which the RDQI > $RDQI_4$ are not included. We presently set $RDQI_4$ = 1 (***rdqi4*** in the aerosol science configuration file).

We now compute the correlation between the 4 x 4 subregion image of each camera to the template image. For each camera, the variance and covariance are calculated as follows:

$$\begin{aligned}
\sigma_k^2 &= \left\langle \rho_k^2 \right\rangle - \left\langle \rho_k \right\rangle^2 \\
\sigma_t^2 &= \left\langle \rho_t^2 \right\rangle - \left\langle \rho_t \right\rangle^2 \\
\sigma_{kt}^2 &= \left\langle \rho_k \rho_t \right\rangle - \left\langle \rho_k \right\rangle \left\langle \rho_t \right\rangle
\end{aligned} \tag{14}$$

where the subscript $k$ refers to camera $k$, the subscript $t$ refers to the template, and the angle brackets indicate a spatial average, computed over the 4 x 4 array of pixels. A straight (unweighted) average is calculated; however, the averaging includes only those pixels for which RDQI ≤ $RDQI_4$. Then, the square of the normalized cross-correlation is calculated as follows:

$$C = \frac{\sigma_{kt}^2 \cdot \left|\sigma_{kt}^2\right|}{\sigma_k^2 \cdot \sigma_t^2} \tag{15}$$

Note that the sign of the covariance between the two windows is preserved in Eq. (15). If there is a high correlation between the equivalent reflectance distribution between the camera $k$ and the template, $C$ takes on values close to 1. Anti-correlation results in negative values of $C$. The criterion for accepting a camera in the subsequent retrievals is that the value of $C$ must exceed a threshold value $C_{thresh}$. This threshold value (***ang_corr_thresh*** in the aerosol science configuration file) is currently set to 0.25 based on experience with this algorithm using in-flight data. If the test fails for any camera, the entire subregion is eliminated. Note that if $\sigma_k^2$, $\sigma_t^2$, or $\sigma_{kt}^2$ in Eq. (15) are zero or close enough to zero to cause a computational problem (this can occur if the equivalent reflectances distributions are uniform), the correlation test is considered to be passed for the affected cameras. The threshold value for this test (***corr_mask_variance_limit*** in the aerosol science configuration file) is currently set to $10^{-6}$.

## 3.4 THEORETICAL DESCRIPTION: STAGE 2 RETRIEVAL PROCESSING

Figure 4 shows those processes which occur at the DAAC prior to the actual aerosol retrievals, in which the processing pathway is chosen dependent on the scene content (referred to as Stage 2). As a first step, input from the Ancillary Geographic Product is used to check the suitability of subregions for application of the heterogeneous land retrieval algorithm. If this is satisfied, the algorithm described in §3.4.2.2 is used to determine whether there are sufficient numbers of cameras and clear subregions to apply the heterogeneous land algorithm. If either the Ancillary Geographic Product or the output of the algorithm in §3.4.3.2 indicates that the heterogeneous land algorithm cannot be applied, a test for the suitability of the dark water retrieval algorithm is applied, as described in §3.4.5.2. If the test passes, the Dark Water algorithm path is chosen. If none of the above conditions is satisfied, the No Retrieval flag is set in the Algorithm Type Flag.

In the following sections, the physical basis of the processes which occur during Stage 2 processing is described, and a mathematical description of the algorithm which is used to implement each process is presented.

### 3.4.1 Search for Dense Dark Vegetation (DDV) subregions

This section is deleted.

*Equation deleted* (16)

*Equation deleted* (17)

*Equation deleted* (18)

*Equation deleted* (19)

### 3.4.2 Check heterogeneous land criteria and calculate processing constraints

In this step, HDRF similar shape constraints are applied, heterogeneous land criteria are checked, and empirical orthogonal functions are calculated.

#### 3.4.2.1 Apply HDRF similar shape constraints

##### *3.4.2.1.1 Physics of the problem*

A simple model of surface directional reflectance that assumes spectral HDRFs can be separated into a function in wavelength multiplied by a function in angle provides powerful constraints on aerosol retrievals performed using multiangle data. This model is based on ATSR-2 heritage and is justified on physical grounds in that the scattering elements which make up most surfaces are large compared to the wavelength of visible and near-infrared light (Flowerdew and Haigh, 1995). We have adapted this algorithm to the multiple looks of MISR (Diner et al., 2005).

##### *3.4.2.1.2 Mathematical description of the algorithm*

The algorithm can be formulated such the surface HDRF is the product of a function that only depends on wavelength and a function that only depends on angle, i.e.,

$$r_\lambda(-\mu,\mu_0,\phi-\phi_0) = a_\lambda f(-\mu,\mu_0,\phi-\phi_0) \tag{19a}$$

The HDRFs $r_\lambda$ in Eq. (7) are a spatial average over the 17.6 km x 17.6 km region corresponding to an aerosol retrieval, excluding contributions from subregions eliminated by cloud masking or other quality filters.

The HDRF divided by its average over camera view is given by

$$r_{camnorm} = \frac{r_\lambda(-\mu,\mu_0,\phi-\phi_0)}{\langle r_\lambda \rangle} = \frac{f(-\mu,\mu_0,\phi-\phi_0)}{\langle f \rangle} \tag{19b}$$

where the angled brackets indicate the angular average. In other words, the HDRF normalized by its camera-averaged value is independent of wavelength. Using a regional estimation of the surface albdedo, $A_\lambda$, the region-averaged HDRF can be expressed as:

$$r_\lambda(-\mu,\mu_0,\phi-\phi_0) = \frac{(1-A_\lambda s_\lambda)\left[\rho_\lambda^{TOA}(-\mu,\mu_0,\phi-\phi_0) - \rho_\lambda^{atm}(-\mu,\mu_0,\phi-\phi_0)\right]}{\left[\exp(-\tau_\lambda/\mu) + t_\lambda(-\mu)\right]\left[e_\lambda^{dir}(\mu_0) + e_\lambda^{diff}(\mu_0)\right]} \tag{19c}$$

where $s_\lambda$ is the bottom-of-atmosphere hemispherical reflectance, $t_\lambda$ is the upwelling diffuse transmittance of the atmosphere, and $e_\lambda^{dir}$, $e_\lambda^{diff}$ are the direct and diffuse downwelling irradiances (normalized by $E_{0\lambda}$) for a black surface, respectively.

Then, $r_\lambda$ normalized by its camera average is given by:

$$r_{camnorm,\lambda} = \frac{r_\lambda(-\mu,\mu_0,\phi-\phi_0)}{\langle r_\lambda \rangle} = \\ = \frac{\left[\rho_\lambda^{TOA}(-\mu,\mu_0,\phi-\phi_0) - \rho_\lambda^{atm}(-\mu,\mu_0,\phi-\phi_0)\right] / \left[\exp(-\tau_\lambda/\mu) + t_\lambda(-\mu)\right]}{constant} \tag{19d}$$

The presumption is that if the correct atmospheric model (that is, the correct aerosol optical depth, single scattering albedo, and phase function) has been selected, $r_{camnorm,\lambda}$ as given by Eq. (19d) is fact be wavelength independent. For an arbitrary atmospheric model, the wavelength independence may not necessarily hold and the degree of departure can be calculated as the variance between $r_{camnorm,\lambda}$ and $\left\{r_{camnorm,\lambda}\right\}$, its band average, which for any wavelength or camera angle is

$$v_{camnorm,\lambda}(-\mu,\mu_0,\phi-\phi_0) = \left[r_{camnorm,\lambda} - \left\{r_{camnorm,\lambda}\right\}\right]^2 \tag{19e}$$

from which an overall residual as a function of aerosol mixture and optical depth is expressed as

$$\chi^2_{angular}(mixture,\tau) = \frac{\sum_\lambda w_\lambda \sum_{cam} q_{cam} v_{camnorm,\lambda}(-\mu,\mu_0,\phi-\phi_0)}{(0.05)^2 \sum_\lambda w_\lambda \sum_{cam} q_{cam}} \tag{19f}$$

where $w_\lambda$ are band weights and $q_{cam}$ are camera weights. The normalizing factor $(0.05)^2$ is inserted in the denominator so that if the difference between $r_{camnorm,\lambda}$ and its band average $\left\{r_{camnorm,\lambda}\right\}$, which are both of order unity, is typically within 5% then the value of $\chi^2_{angular}$ will be on the order of unity. Bands 1-4 (blue, green, red, and near-infrared) are assigned $w_\lambda$ values of 4, 3, 2, and 1 respectively; that is, departures from the common angular shape are more heavily penalized at the shorter wavelengths. Sensitivity to errors in the atmospheric model is expected to be greater in the blue because optical depth increases as wavelength decreases for most aerosols. Similarly, the camera weights, $q_{cam}$, are set equal to the inverse of the cosine of the camera's view zenith angle to take advantage of the greater atmospheric sensitivity of the oblique views.

A computational subtlety is noted here. It is possible, according to Eq. (19d), for the value of $r_{camnorm,\lambda}$ to take on a negative value, if a particular aerosol mixture/optical depth combination is not correct, e.g., if the optical depth is too large. To penalize such unphysical

situations, we calculate the variance in accordance both with Eq. (19e) and also by replacing $r_{camnorm,\lambda}$ by its absolute value. The variance used in Eq. (19f) is the larger of the two values.

An alternative way of viewing the surface model implied by Eq. (19a) is to calculate the HDRF divided by its band-averaged value, denoted by curly brackets, given by

$$r_{bandnorm,\lambda} = \frac{r_\lambda(-\mu,\mu_0,\phi-\phi_0)}{\{r_\lambda(-\mu,\mu_0,\phi-\phi_0)\}} = \frac{a_\lambda}{\{a_\lambda\}} \tag{19g}$$

In this formulation, the HDRF normalized by its band-averaged value is independent of angle. For a particular assumption about the aerosol type and amount we can quantify the departure in the HDRF calculated by Eq. (19c) from this condition. This is done by first defining a variance, given by

$$v_{bandnorm,\lambda}(-\mu,\mu_0,\phi-\phi_0) = \left[r_{bandnorm,\lambda} - \langle r_{bandnorm,\lambda}\rangle\right]^2 \tag{19h}$$

from which an overall spectral residual is derived:

$$\chi^2_{spectral}(mixture,\tau) = \frac{\sum_\lambda w_\lambda \sum_{cam} q_{cam} v_{bandnorm,\lambda}(-\mu,\mu_0,\phi-\phi_0)}{(0.05)^2 \sum_\lambda w_\lambda \sum_{cam} q_{cam}} \tag{19i}$$

In principle, the aerosol mixture and optical depth that minimizes either Eq. (19f) or Eq. (19i) would be the "best" aerosol model. In practice, Eq. (19a) probably does not hold exactly, and it is possible that minimization of the cost function in Eq. (19f) is the better algorithm, or alternatively, minimization of Eq. (19i) is better. Therefore, the algorithm was designed to provide a weighted linear combination of the two cost functions (angular and spectral) as the overall residual, i.e.,

$$\chi^2_{shape}(mixture,\tau) = \beta\chi^2_{angular} + (1-\beta)\chi^2_{spectral} \tag{19j}$$

Both the angular and spectral approaches worked reasonably well under testing, one giving better results over some targets than the other and vice versa. Since we could not identify any obvious physical reason to choose one formulation over the other, the value of β has been set to 0.5.

The constraints are determined as follows. Using the set of prescribed aerosol mixtures and the grid in optical depth, the function $\chi^2_{shape}(mixture,\tau)$ is calculated as described above. The value $\chi^2_{globalminimum}(mixture,\tau)$, the minimum value of this function over the entire two-dimensional mixture/optical depth grid, is then determined. For a particular mixture, if there is no optical depth for which $\chi^2_{shape}(mixture,\tau) \le f_{mix} \cdot \chi^2_{globalminimum}(mixture,\tau)$, where $f_{mix}$ is a threshold factor greater than unity, that mixture is eliminated. Next, for each surviving mixture,

the value $\chi^2_{mixtureminimum}(mixture,\tau)$, the minimum value of the residual for that mixture, is determined. Any optical depth for which $\chi^2_{shape}(mixture,\tau) \le f_{tau} \cdot \chi^2_{mixtureminimum}(mixture,\tau)$, where $f_{tau}$ is another threshold factor greater than unity, is considered to be an acceptable candidate optical depth for that mixture. Essentially this procedure says that there is some set of mixtures, and range of optical depths for each mixture, for which the residuals are within some factor of the residuals obtained for those aerosol models that best satisfy the HDRF angular/spectral shape similarity criterion established by Eq. (19a). Note that this process seeks those aerosol models for which the angular and spectral shapes are most similar, without requiring that they be precisely identical. Thus, the algorithm works as long as the model represented by Eq. (19a) is approximately true. Following testing, the values of $f_{mix}$ and $f_{tau}$ were both set to 2.0, and represented as ***hdrf_thresh_factor_mix*** and ***hdrf_thresh_factor_tau,*** respectively, in the aerosol science configuration file. An additional test checks to ensure that the value of $\chi^2_{shape}(mixture,\tau)$ does not exceed a certain threshold, ***max_chisq_homog_thresh*** in the aerosol science configuration file, currently set to 10.0.

The per-band retrieval results are stored as ***OptDepthHomogCalcPerBand*** and ***ChisqHomogCalcPerBand***. The spectral and geometric weights, ***frac_geom_spec_mix*** and ***frac_geom_spec_tau***, are set in the aerosol science configuration file, as are the multiplying factors ***hdrf_thresh_factor_mix*** and ***hdrf_thresh_factor_tau***. An additional parameter, ***num_tau_extra***, is also specified in the configuration file. When the shape similarity mask results in the number of available points on the fine optical depth grid being equal to 1 for a particular mixture, the window of available $\tau$ values is expanded by ***num_tau_extra*** grid points in the higher $\tau$ direction. The purpose of this step is to deal with possible underestimation of optical depth in low aerosol loading conditions.

The result of this process is a mixture/optical depth "mask" flagging those mixtures and candidate optical depths which survive the above tests. Then, for any surviving mixture and acceptable candidate range of optical depths within that mixture, we apply the HetSurf algorithm described in §3.5.5.2.3. Without the mask, HetSurf would be applied to all mixtures and optical depths; the mask constrains the allowable set of mixtures and optical depths. The conditions of success for the HetSurf algorithm are applied to this constrained set of mixture/optical depth combinations.

The minimized residual $\chi^2_{homog}$, determined from the residuals $\chi^2_{shape}$ defined by Eq. (19j), is archived in the aerosol product as ***ChisqHomog***.

#### 3.4.2.2 Check heterogeneous land criteria

##### *3.4.2.2.1 Physics of the problem*

Contrast in the surface reflectances is required for the EOF portion of the algorithm. Regions which do not contain sufficient contrast are screened out here.

#### *3.4.2.2.2 Mathematical description of the algorithm*

Calculation of the EOFs and application of the subsequent retrieval algorithm is done for all available bands for which certain conditions are met. For each band individually we require:

(1) That at least one subregion within the 17.6-km region is designated as Land in the AGP;

(2) That the subregions used in the retrieval are classified as Clear;

(3) That the subregions used in the retrieval must be viewed in common by all available cameras and bands to be used by the algorithm, and that the common number of subregions (***min_het_subr_thresh*** in the aerosol science configuration file) is ≥ at least 16;

(4) That all subregions used in the retrieval must be viewed by at least two forward-looking cameras, of which at least one is Cf or Df and of which at least one is Af or Bf, and at least two aftward-looking cameras, of which at least one is Ca or Da and of which at least one is Aa or Ba, and at least one nadir- or near-nadir-looking camera, of which one is An, Aa, or Af;

(5) That a region angular correlation test is passed, in a similar manner as described in §3.3.8.2.10 but instead using 16 x 16 arrays of 1.1-km red band equivalent reflectances and creating a template image using only the An, Aa, and Af cameras, and using a correlation threshold of 0.1 and a variance threshold of $10^{-8}$ (***reg_ang_corr_thresh*** and ***reg_corr_mask_variance_limit*** in the aerosol science configuration file).

(6) That this band is to be used in the retrieval (as specified by ***het_band_mask*** in the aerosol science configuration file).

Additionally, there must be usable data in the filter band, currently set to the red band (***het_filter_band*** in the aerosol science configuration file), and the weighted mean radiance of each subregion must pass a threshold test (currently disabled), where the weighted mean radiance $\overline{\rho_w}$ is defined as

$$\overline{\rho_w} = \frac{\sum_k \frac{1}{\mu_k} \cdot \rho_k}{\sum_k \frac{1}{\mu_k}} \tag{19k}$$

where the subscript $k$ refers to camera $k$, the weights $1/\mu_k$ are the inverse of the cosine of the camera view angle, and $\rho_k$ is the 1.1 km equivalent reflectance. The threshold test is

$$\overline{\rho_w} < (\min(\overline{\rho_w}) + \left\langle \overline{\rho_w} \right\rangle_{thresh} \cdot (\max(\overline{\rho_w}) - \min(\overline{\rho_w}))) \tag{19l}$$

where $\left\langle \overline{\rho_w} \right\rangle_{thresh}$ is ***het_land_radiance_thresh*** in the aerosol science configuration file. The threshold is currently set to 1.0, which turns off the test. The minimum weighted mean radiance value in a region is archived in the aerosol product for all channels as ***RegEqReflDarkest.***

If these conditions are met, these subregions, cameras, and bands are used in the EOF calculation and in the retrieval, and the ***AlgTypeFlag*** field in the aerosol product indicates that the heterogeneous retrieval is used. Otherwise, this region is not suitable for the heterogeneous land algorithm.

#### 3.4.2.3 Calculate empirical orthogonal functions

##### *3.4.2.3.1 Physics of the problem*

The concept behind this step of the heterogeneous land aerosol retrieval is to constrain the angular shape of the surface-leaving radiation field (Martonchik and Diner, 1992). The constraints to be derived at this stage of the processing take the form of empirical orthogonal functions (EOFs), determined from an analysis of the angular shape characteristics of the TOA equivalent reflectances of the various heterogeneous samples in the region for which the retrieval is being done. The heterogeneous land retrieval algorithm then uses these EOFs to represent the sample-averaged surface-leaving reflectances for the region. Since the sample-averaged TOA equivalent reflectance is dependent on both the sample-averaged surface-leaving reflectance and the atmospheric path radiance this processing step serves as a precursor to the solution for the best-fitting aerosol model, described below. If the land aerosol retrieval is unsuccessful, a dark water retrieval is attempted.

##### *3.4.2.3.2 Mathematical description of the algorithm*

Regions 17.6 km x 17.6 km in size (i.e., 16 x 16 1.1-km samples) are analyzed under the assumption that 1-D radiation transfer, described by Eq. (2), is valid. The EOFs required to implement the heterogeneous land aerosol retrieval are the eigenvectors associated with the real, symmetric scatter matrix constructed from reduced sample equivalent reflectances, defined to be sample TOA equivalent reflectances minus the sample-averaged TOA equivalent reflectance. This subtraction removes the atmospheric path radiance, which is assumed to be the same for each sample in the region. The construction of the EOFs is done on each spectral band individually.

A reduced sample equivalent reflectance at subregion location *x, y* is computed for each camera view angle and each band,

$$J_{x,y}(\mu,\mu_0,\phi-\phi_0) = \rho_{x,y}(\mu,\mu_0,\phi-\phi_0) - \rho_{bias}(\mu,\mu_0,\phi-\phi_0), \tag{20}$$

where $\rho_{bias}$ denotes an offset equivalent reflectance. The explicit band dependence of Eq. (20) and all subsequent equations in this section has been suppressed for simplicity. The algorithm for establishing $\rho_{bias}$ is to find that particular subregion with the minimum value of equivalent reflectance in the green band and for the nadir camera, from among the common subregions. If the green band is not available, then the red band is used, followed in preference by the blue band. If the nadir camera is not available, then the camera closest to the nadir view is selected, i.e., that camera with a cosine of the view zenith angle $\mu$ closest to 1. Once this particular minimum equivalent reflectance subregion is found, its associated equivalent reflectances for all cameras and bands are used as the offset reflectances $\rho_{bias}$ in Eq. (20).

Each $J_{x,y}$ is a sample-dependent linear combination of the spatially variable component of the TOA sample equivalent reflectance, called surface functions [see Eq. (70)]. The scatter matrix (Preisendorfer, 1988) then is defined as

$$C_{i,j} = \frac{1}{N_{sub}} \sum_{x,y} J_{x,y,i} \cdot J_{x,y,i} \tag{21}$$

where the indices *i* and *j* are used to denote the viewing geometry and $N_{sub}$ is the number of summed-up subregions. The scatter matrix is a $N_{cam}$ x $N_{cam}$ element array, where $N_{cam}$ is the number of available cameras (nominally, 9) in the particular spectral band being analyzed, with $\mu_i, \phi_i$ defining the view geometry of MISR camera *i*. The eigenvectors of *C* are solutions to the eigenvector equation given by

$$\sum_{j=1}^{N_{cam}} C_{i,j} \cdot f_{j,n} = \lambda_n \cdot f_{i,n} \tag{22}$$

where $\lambda_n$ is the eigenvalue (real and positive) of $f_{i,n}$. In general there will be $N_{cam}$ eigenvalue and eigenvector solutions with the $N_{cam}$-element eigenvectors forming an orthonormal set, i.e.,

$$\sum_{i=1}^{N_{cam}} f_{i,n} \cdot f_{i,m} = \delta_{nm} \tag{23}$$

where $\delta_{nm}$ is the Kronecker delta. Thus, every $N_{cam}$-element vector $J_{x,y}$ can be expanded in terms of this orthonormal set as

$$J_{x,y,i} = \sum_{n=1}^{N_{cam}} A_n^{x,y} \cdot f_{i,n} \tag{24}$$

where $A_n^{x,y}$ are the principal components,

$$A_n^{x,y} = \sum_{i=1}^{N_{cam}} J_{x,y,i} \cdot f_{i,n} \tag{25}$$

obtained by applying the orthonormality condition of Eq. (23) to Eq. (24).

The eigenvectors are ordered according to the magnitude of the corresponding eigenvalues, i.e., $\lambda_1 > \lambda_2 > ... > \lambda_{N_{CAM}}$. The set of vectors $f$ is the optimum basis function set to represent the vectors $J_{x,y}$ in the sense that if only the $N < N_{cam}$ eigenvectors are used in the expansion, then the resulting error $e$ is a minimum when compared to the error using first $N$ vectors from a different vector basis function set. The error is defined as

$$e = \frac{1}{N_{sub}} \sum_{x,y} \sum_{i=1}^{N_{cam}} \left( J_{x,y,i} - \sum_{n=1}^{N} A_n^{x,y} \cdot f_{i,n} \right)^2$$

$$= \frac{1}{N_{sub}} \sum_{x,y} \sum_{i=1}^{N_{cam}} \left( \sum_{n=N+1}^{N} A_n^{x,y} \cdot f_{i,n} \right)^2 = \sum_{n=N+1}^{N_{cam}} \lambda_n \qquad (26)$$

This basis function set should also be the optimum orthonormal set to expand the sample-averaged TOA equivalent reflectance minus the atmospheric path term since all reduced equivalent reflectances are composed of the same surface functions as expressed in Eq. (70). Further discussion, and a demonstration of this technique using Advanced Solid-state Array Spectroradiometer (ASAS) aircraft data is given in (Martonchik, 1997).

*Equation deleted* (27)

*Equation deleted* (27a)

*Equation deleted* (28)

*Equation deleted* (29)

*Equation deleted* (30)

*Equation deleted* (31)

### 3.4.3 Determine minimum equivalent reflectances (heterogeneous land)

#### 3.4.3.1 Physics of the problem

The purpose of this process is to constrain the upper bound of spectral optical depth for the clear (optically thin) retrieval paths over heterogeneous land. For each 17.6 km square region composed of 1.1-km samples, the first step is to find the smallest observed equivalent reflectance for each spectral band at each camera angle. The darkest samples in the region are used to constrain the maximum allowable amount (in terms of optical depth) of a given type of aerosol; a greater amount of that type of aerosol would require the physical impossibility of negative surface reflectivities in order to reproduce the observed TOA equivalent reflectance (see §3.5.4). Knowledge of the minimum spectral equivalent reflectances obviously provides a useful constraint on later steps in the aerosol retrieval process and the resulting maximum clear-sky optical depths are themselves valuable indicators of maximum aerosol amount.

#### 3.4.3.2 Mathematical description of the algorithm

The algorithm finds the minimum equivalent reflectances in the four spectral bands at each camera angle in a region of 16 x 16 samples, each 1.1 km in size, using only samples marked Clear. Simple inequality tests are used

### 3.4.4 Determine band-differenced optical depth (heterogeneous land)

This section is deleted.

*Equation deleted* (32)

*Equation deleted* (33)

*Equation deleted* (34)

*Equation deleted* (35)

*Equation deleted* (36)

*Equation deleted* (37)

*Equation deleted* (38)

### 3.4.5 Search for Dark Water (DW) subregions

#### 3.4.5.1 Physics of the problem

The purpose of this step is to determine if the dark water aerosol retrieval should be applied to a region.

#### 3.4.5.2 Mathematical description of the algorithm

A region is considered suitable for the dark water algorithm if at least ***min_dw_subr_thresh*** common subregion locations are usable across ***min_dw_cam_thresh*** cameras. A subregion is usable, for a given camera, if the following criteria are met:

(1) The subregion location is designated as Deep Ocean or Deep Inland Water in the AGP;

(2) The subregion is classified as Clear in all required bands. Required bands are Red and Near-Infrared, plus any additional bands specified by the ***dw_band_mask*** in the aerosol science configuration file.

Given the set of usable subregions for each camera, find the largest set of cameras with at least ***min_dw_subr_thresh*** subregions in common. If at least ***min_dw_cam_thresh*** cameras can be found which have the required ***min_dw_subr_thresh*** subregions in common then the region is suitable for the dark water algorithm. The set of at least ***min_dw_cam_thresh*** cameras and common usable subregion locations across those cameras are subsequently used in section

3.5.1.2.1.

## 3.5 THEORETICAL DESCRIPTION: STAGE 3 RETRIEVAL PROCESSING

During this stage, aerosol retrievals are performed for the various 17.6-km x 17.6-km regions. Retrievals consist of determining the "goodness of fit" of a set of aerosol models to the MISR observations, based on a set of criteria described below. The set of candidate models is established by referencing the Aerosol Climatology Product, and each in turn is compared with the MISR data. The processing steps described in §3.5.3 through §3.5.8 are repeated for each aerosol model to be tested during the retrieval. The retrieval results, including goodness-of-fit parameters and other retrieval flags, will be reported in the Aerosol/Surface Product for all candidate models. However, only those models for which the goodness-of-fit parameters satisfy pre-established criteria are deemed "successful" retrievals. Whether a single model or multiple models provide suitable fits to the data depends on the ambient atmospheric conditions, the view and solar geometry, and the completeness of the ACP and SMART databases. Among the successful models, the minimum and maximum optical depths provide a measure of uncertainty of the "best estimate" optical depth reported in the Aerosol/Surface Product.

During retrievals, MISR band 2 (green) is used as a reference band. This means that when stepping through various values of optical depth to find the best-fitting value for a particular aerosol model, the band 2 optical depth is the independent variable. Optical depths in the other MISR bands are appropriately scaled, using the spectral extinction cross sections of the models contained in the ACP. Band 2 is used because its effective wavelength (558 nm) is closest to the reference wavelength commonly used by the aerosol community. After retrievals are performed, optical depth results are reported for this band. The user may convert the reported optical depths to other bands by making use of the spectral extinction cross section data contained in the ACP.

### 3.5.1 Establish equivalent reflectances for retrieval

#### 3.5.1.1 Physics of the problem

This step involves establishing the equivalent reflectances corresponding to the MISR observations that will be used during the retrievals. The methodology depends on the retrieval pathway chosen in Stage 2.

#### 3.5.1.2 Mathematical description of the algorithm

##### *3.5.1.2.1 Dark water*

At each 1.1-km subregion location, calculate the average equivalent reflectance of the red and near-infrared band across the set of cameras selected in section 3.4.5.2. Choose the subregion location which has the minimum of this average to be the common subregion used for the Dark Water retrieval. The equivalent reflectance at this common subregion is also used to

calculate the optical depth upper bound for the dark water algorithm.

The equivalent reflectances at this location are archived in the aerosol product as ***RegEqRefl***, and ***NumAcceptSubr*** is set to 1. The standard deviations of the equivalent reflectances for the entire set of common subregions is archived as ***RegEqReflStDev***. The selected common subregion is archived as ***SubrUsed***.

#### *3.5.1.2.2 Heterogeneous land*

For the heterogeneous land retrieval algorithm, the retrieval incorporates a selectable set of bands and the common subregions between cameras as determined in §3.4.2.2. A spatial average of the subregion equivalent reflectances within each camera and band is needed by the algorithm. The mean equivalent reflectances are archived in the aerosol product as ***RegEqRefl***, the standard deviations of the equivalent reflectances are archived as ***RegEqReflStDev***, and the number of subregions used is archived in the aerosol product as ***NumAcceptSubr***.

### 3.5.2 Establish aerosol models

The aerosol models to be compared with MISR observations during the retrievals consist of tropospheric models generated from mixtures of the pure particles contained in the ACP. The ACP also defines which mixtures are to be used for each of the aerosol retrieval pathways (dark water or heterogeneous land). Each tropospheric mixture contains up to three pure particles, and the relative abundances are specified in the ACP.

Relative abundances of the components are defined in the ACP in terms of fraction of total optical depth (not by numbers of particles). Since these relative abundances are wavelength dependent, due to the dependence of extinction cross section on wavelength, the ACP provides the fractional optical depth mixing ratios at each wavelength.

### 3.5.3 Determine model TOA equivalent reflectances

#### 3.5.3.1 Physics of the problem

This section describes how the model TOA equivalent reflectances used as the basis of the aerosol retrievals are calculated. A principal input to this process is the SMART Dataset, which contains information on a standard optical depth grid. This grid is identical in all four MISR bands. The model TOA equivalent reflectances described in this section are calculated at each wavelength used in the retrievals on this optical depth grid. Once this set of values has been established, they will then be interpolated to a finer optical depth grid for the purpose of computing the residuals between the model and observed TOA equivalent reflectances as a function of optical depth, in order to find the optical depth that minimizes these residuals for each aerosol model. This interpolation and the calculation of the residuals are described later, in §3.5.5.

##### *3.5.3.1.1 Dark water*

For aerosol models consisting of the pure particles contained in the ACP, components of the TOA equivalent reflectances are obtained from the SMART Dataset, with the surface component provided using an assumed wind-speed-driven glitter and whitecap model. It is then required to interpolate the data in the SMART Dataset to the correct observing and illumination geometry.

For aerosols comprised of mixtures of several pure particle types, calculations based on the SMART Dataset input are required to establish the TOA equivalent reflectances. These are obtained during the retrievals, using a modified form of linear mixing theory. Standard linear mixing states that TOA equivalent reflectance for a mixture of particles having a particular total optical depth can be approximated by summing the TOA equivalent reflectances for the individual aerosol components, evaluated at the total optical depth value, but weighted in the summation by that component's relative abundance (as a fraction of the total extinction optical depth). This approximation is exact in the single-scattering limit, and works well for multiple scattering mixtures of conservatively and mildly absorbing particles. However, when a component is highly absorbing, the linear mixing approximation consistently overestimates the TOA equivalent reflectances. To account for this, a new method has been developed, which generalizes linear mixing to include absorbing particles.

#### *3.5.3.1.3 Heterogeneous surface*

The heterogeneous surface retrieval approach makes use of the black surface radiation fields provided in the SMART Dataset, interpolated to the appropriate geometries. Modified linear mixing theory is used to generate aerosol mixtures.

### 3.5.3.2 Mathematical description of the algorithm

#### *3.5.3.2.1 Pure aerosol TOA equivalent reflectance calculations*

As described above, the required pure aerosol TOA equivalent reflectances for the dark water and heterogeneous land retrieval pathways are obtained from the SMART Dataset.

*Equations deleted* (39-58)

#### *3.5.3.2.2 Nearest neighbor and interpolative assignments of parameter values*

Each region over which aerosol retrievals are performed will have a set of $\mu$ and $\phi - \phi_0$ values associated with each camera, and a single value of $\mu_0$. Multiple-scattered TOA equivalent reflectances are provided in the SMART Dataset on a predetermined geometric grid, and interpolation is necessary. The equivalent reflectance fields in the SMART Dataset are provided on a grid in $\mu$, $\mu_0$, and $\Omega$, rather than $\mu$, $\mu_0$, and $\phi - \phi_0$. This is done so that the grid in $\Omega$ can be tailored to provide fine enough sampling in the rainbow region, where the single-scattering phase functions of large, spherical particles vary considerably. The same $\mu$, $\mu_0$, and $\Omega$ grid is used for all aerosol types. Because of the one-to-one correspondence between $\phi - \phi_0$ and $\Omega$, expressed by Eq. (11), quadratic interpolation of the SMART equivalent reflectances over each of the

variables $\mu$, $\mu_0$, and Ω provides the required data at the values of $\mu$, $\mu_0$, and ϕ - $\phi_0$ required for a given camera.

Additional assignments of parameter values to be used in the retrievals are performed as follows:

(1) For dark water retrievals, use SMART equivalent reflectances for the wind speed closest to the ambient wind speed.

(2) For all retrievals, use SMART-provided quantities, which are provided at two values of atmospheric pressure, and linearly interpolate to the ambient surface pressure at the mean terrain altitude of the 17.6-km region.

#### *3.5.3.2.3 Aerosol mixture TOA equivalent reflectance calculations*

The retrieval process requires determination of equivalent reflectance of aerosol mixtures in terms of the equivalent reflectances of the pure particles comprising the mixture. In principle, the most exact way to do this is to perform the appropriate radiative transfer calculations for the aerosol mixture and store the results in the SMART Dataset. However, in order to provide operational flexibility in case it is determined that a different set of mixtures should be used, and to minimize the required storage space for the SMART Dataset, an approximation which requires knowledge of only the pure particle optical properties and equivalent reflectances is utilized.

The approximation used is a generalization of the linear mixing approach. For a given total optical depth τ of an aerosol mixture containing *n* components, standard linear mixing states that:

$$\rho_{mixture}(-\mu,\mu_0,\phi-\phi_0;\tau)=\sum_n f_n\rho_n(-\mu,\mu_0,\phi-\phi_0;\tau) \tag{59}$$

where $\rho_{mixture}$ is the TOA equivalent reflectance for the aerosol mixture, $\rho_n$ is the TOA equivalent reflectance for the *n*th aerosol component, and $f_n$ is the relative abundance of the $n^{th}$ aerosol component. Note that the equivalent reflectances for each aerosol component contain all contributions due to Rayleigh scattering or other atmospheric constituents common to each of the pure aerosol cases. Equation (59) is exact in the single scattering limit, but significantly overestimates the TOA equivalent reflectances when one or more of the aerosol components is highly absorbing. The following equation provides a much better approximation:

$$\begin{aligned}\rho_{mixture}(-\mu,\mu_0,\phi-\phi_0;\tau)=&\\ &\rho^{black}_{R,ms}(-\mu,\mu_0,\phi-\phi_0;\tau_R)+\\ &+\sum_n f_n\rho^{black}_{n,ss}(-\mu,\mu_0,\phi-\phi_0;\tau)+\end{aligned}$$

$$+\sum_n f_n \frac{\varpi_{mix}}{\varpi_n} e^{-\tau|\varpi_{mix}-\varpi_n|}[\rho^{black}_{n,ms}(-\mu,\mu_0,\phi-\phi_0;\tau)-\rho^{black}_{R,ms}(-\mu,\mu_0,\phi-\phi_0;\tau_R)]+$$

$$+\sum_n f_n \rho_{n,surf}(-\mu,\mu_0,\phi-\phi_0;\tau) \qquad (60)$$

where $\rho^{black}_{n,ss}$ is the TOA equivalent reflectance resulting from single-scattered radiation over a black surface (including the contributions from both Rayleigh scattering and aerosol particle *n*), $\rho^{black}_{n,ms}$ is the multiple-scattered field under the same conditions, $\rho^{black}_{R,ms}$ is the pure Rayleigh multiple-scattered field over a black surface, $\tau_R$ is the Rayleigh optical depth, $\varpi_n$ is the single scattering albedo of the *n*th pure aerosol component (obtained from the ACP), $\varpi_{mix}$ is the single scattering albedo for the mixture (also obtained from the ACP), and $\rho_{n,surf}$ is the component of the TOA radiation field involving interactions with the surface, for aerosol particle *n*. For the dark water retrievals, $\rho_{n,surf}$ is obtained from the SMART Dataset.

As mentioned previously, the terms in Eq. (60) which are obtained from the SMART Dataset are stored there as functions of $\mu$, $\mu_0$, and $\Omega$ for practical reasons. However, we make use of the correspondence between $\Omega$ and $\phi$ - $\phi_0$ in showing the terms in Eq. (60) as explicit functions of $\mu$, $\mu_0$, and $\phi$ - $\phi_0$.

Equation (60) preserves the standard linear mixing formulation for single-scattered radiation and for radiation which has interacted with the surface. It reduces the magnitude of the multiple-scattered field in the path radiance field when absorbing aerosols are present. Application of this modified linear mixing equation to the path radiance has been tested for all combinations of aerosols contained in the ACP, and provides accurate results for all cases up to total aerosol optical depths of at least 2.

### 3.5.4 Determine optical depth upper bound

#### 3.5.4.1 Physics of the problem

This step is performed for each candidate aerosol model. The algorithm to determine the upper bound on optical depth is the same whether the region is dark water or heterogeneous land. It uses the TOA equivalent reflectances assuming a nearly-black surface in a straightforward manner to find the optical depth of the particular model being tested that corresponds to the minimum equivalent reflectances calculated during the Stage 2 processing.

#### 3.5.4.2 Mathematical description of the algorithm

The optical depth upper bound is computed as follows:

(1) Using the pixels appropriate for the retrieval type, for each camera that is available, and for each available band within a given camera, take the model black surface TOA equivalent reflectances as a function of optical depth, and

add a limiting surface reflectance contribution to it (see Eq. (60a) below).

(2) Linearly interpolate these values to find the optical depth in each of the available channels that corresponds to the observed minimum equivalent reflectance (found in §3.4.3 for heterogeneous land, and 3.5.1.2.1 for water) in the same channel;

(3) Repeat steps (1) and (2) for all cameras;

(4) Given the set of optical depths determined from the above steps (up to 36 values), the optical depth upper bound is established as the minimum value in this set for land, or the maximum value for water, as determined by the aerosol science configuration file flags ***land_maxval_flag*** and ***water_maxval_flag***. The maximum value is used for water because simulation tests showed that otherwise the correct model was sometimes eliminated because the minimum $\tau$ upper bound was too restrictive.

The limiting surface contribution which is added to the model black surface TOA equivalent reflectance is given by:

$$\left(\rho_{surface}\right)_{limiting} = \left(e^{-\tau/\mu} + t_{diff}\right) \cdot albedo_{thresh} \cdot \left(\mu_0 e^{-\tau/\mu_0} + e_{diff}\right) \tag{60a}$$

where $e^{-\tau/\mu} + t_{diff}$ is the direct and diffuse transmittance from the surface, $\mu_0 e^{-\tau/\mu_0} + e_{diff}$ is the direct and diffuse irradiance at a black surface, and $albedo_{thresh}$ is ***albedo_thresh_land*** or ***albedo_thresh_water*** (depending on underlying surface type) in the aerosol science configuration file. Currently ***albedo_thresh_land*** is set to 0.015, and ***albedo_thresh_water*** is set to 0.0 (turned off). The optical depth upper bound, and the camera and band which established it, are archived in the aerosol product for each candidate aerosol model as ***OptDepthUpBd***, ***OptDepthUpBdCam***, and ***OptDepthUpBdBand***.

### 3.5.5 Compute residuals as a function of optical depth

The computation of residuals differs depending on the retrieval algorithm type. The following sections describe the physics of the problem for each type, followed by a mathematical description of the algorithm. Clear scenes for which the surface reflectance is not dark water or heterogeneous land [as defined by the Eq. (31)] are not currently being dealt with.

The residuals derived below are defined to be functions of optical depth in MISR band 2 (558 nm) as the independent variable. For a particular aerosol model, the best-fitting optical depth is the one that minimizes the parameters $\chi^2_{abs}$ (***ChisqAbs***) for dark water, and $\chi^2_{het}$ (***ChisqHet***) for heterogeneous land. These parameters, defined below, provide measures of the residuals between the model and observed TOA equivalent reflectances. In order to find the optical depth that minimizes these residuals, we compute them as a function of optical depth on a

fine grid. The model TOA equivalent reflectances calculated in §3.5.3 are established at optical depth values corresponding to the grid contained in the SMART Dataset. We use quadratic interpolation to determine equivalent reflectances at optical depths on a finer grid, to insure that the value that minimizes the residuals is not missed.

After the best-fitting optical depth for each aerosol model is found, additional residuals, known as $\chi^2_{geom}$, $\chi^2_{spec}$, and $\chi^2_{maxdev}$ are calculated for the dark water retrievals. These additional parameters are used as discriminants of the goodness-of-fit of a particular aerosol model to the MISR observations. They are evaluated at the best-fitting optical depth by interpolating the equivalent reflectances determined in §3.5.3 on the SMART Dataset optical depth grid to this value and performing the requisite calculations.

Additional residuals and optical depths are computed using each spectral band separately, for each algorithm type. The per-band results for the heterogeneous surface algorithm are used as a constraint in the heterogeneous surface aerosol retrieval.

Additional residuals are computed which combine the $\chi^2$ residuals from each retrieval type with the optical depth uncertainties. These combined residuals are used to determine which single aerosol model was the best fit to the observations.

It is important to note that the mathematical definitions of the residuals include summations over wavelength of various model terms, such as equivalent reflectances. Thus, while stepping through the fine grid of optical depth values in the reference band (band 2), it is necessary to determine the optical depth at the other MISR wavelengths at which the model terms included in the summations are to be calculated. Because optical depth depends on wavelength, and this dependence varies from one aerosol model to another, spectral scaling factors provided by the ACP are used to determine the appropriately scaled optical depths in bands 1, 3, and 4.

#### 3.5.5.1 Physics of the problem

##### *3.5.5.1.1 Dark water*

Having specified surface wind speed, and given the view/solar geometry corresponding to a particular measurement, the TOA equivalent reflectances in the 446 nm, 558 nm, 672 nm and 866 nm MISR channels are determined at each camera angle for each of the aerosol compositional mixture/size distribution models to be tested. The predicted equivalent reflectances for each model and optical depth value are compared with the actual MISR observations and various residuals between them are calculated. The contributions from the 446 nm and 558 nm channels are weighted by optical depth, while the contributions from the 672 nm and 866 nm channels are used fully. A single retrieval will be performed over a 17.6 km x 17.6 km region, using measured equivalent reflectances as determined in §3.5.1.2.1.

##### *3.5.5.1.2 Heterogeneous surface*

Finding the residuals for heterogeneous surface requires a different strategy than used for the dark water cases. The goodness-of-fit criterion to be applied is that the angular shape of the sample-averaged TOA equivalent reflectance (from all available samples in a 17.6 km x 17.6 km region) minus the atmospheric path term (the component of the radiation field which is back scattered to space without interacting with the surface) must be similar in a least squares sense to a linear combination of EOFs (fewer than nine), generated from the TOA equivalent reflectances only (see §3.4.3.2). It can be shown that if all samples within the region have the same angular shape of their bidirectional reflectance factors, or BRFs, (albeit different albedos in order to pro vide surface contrast), this criterion can be satisfied exactly if the "correct" aerosol model is assumed. The basis of this MISR retrieval algorithm is to assume that the same goodness-of-fit criterion holds even in the more realistic case where both albedo and bidirectional reflectance vary from sample to sample. The effectiveness of this method under this generalized case was demonstrated theoretically (Martonchik and Diner, 1992) and the algorithm was used in the analysis of ASAS airborne, multi-angle imagery (Martonchik and Conel, 1994).

#### 3.5.5.2 Mathematical description of the algorithm

##### *3.5.5.2.1 Dark water*

The criterion to be used to find the best-fitting optical depth is minimization of the reduced $\chi^2_{abs}$ parameter, calculated as a function of optical depth as follows:

$$\chi^2_{abs}(\tau) = \frac{\sum_{l=1}^{4} w_l \cdot \left[ \sum_{j=1}^{9} w_j \cdot \nu(l,j) \cdot \frac{\left[\rho_{MISR}(l,j) - \rho_{model}(l,j)\right]^2}{\sigma^2_{abs}(l,j)} \right]}{\sum_{l=1}^{4} w_l \cdot \left[ \sum_{j=1}^{9} w_j \cdot \nu(l,j) \right]} \tag{61}$$

where $\rho_{MISR}$ are MISR equivalent reflectances, computed by taking the darkest subregion in the 17.6 km x 17.6 km region which passed through all screens, $\rho_{model}$ are the model TOA equivalent reflectances for the aerosol mixture, and $\sigma_{abs}$ is the absolute radiometric uncertainty in $\rho_{MISR}$. The sum over *j* corresponds to the cameras and the sum over *l* corresponds to wavelength. The parameter $\nu(l,j)$ = 1 if a valid value of $\rho_{MISR}(l,j)$ exists; otherwise = 0. Eq. (61) also contains weighting factors $w_j$. For the dark water retrievals, $w_j$ is 1 where data are present, and 0 elsewhere. The value of $\sigma_{abs}(l,j)$ is obtained as follows:

$$\sigma_{abs}(l,j) = 0.05 \max\left(\rho_{MISR}(l,j), 0.04\right) \tag{61a}$$

The $w_l$ values are per-band weights which vary linearly from 0 to 1 between optical depth lower and upper thresholds (***dw_tau_min_for_weights, dw_tau_max_for_weights*** in the aerosol science configuration file). The per-band weights are equal to 0 below the optical depth lower threshold, and equal to 1 at or above the optical depth upper threshold. These weights allow individual bands to contribute varying amounts to the $\chi^2_{abs}$ minimization as a function of optical

depth. Since the dark water surface is assumed to have negligible reflectance in bands 3 and 4, the weights are configured to allow full use of these channels at all optical depths. However, contributions in the blue and green channels, where the dark water surface reflectance is non-negligible, are not included in the minimization below optical depths of 0.75 and 0.50 in bands 1 and 2 respectively. As the aerosol optical depth increases above these levels, the relative surface contribution to the overall equivalent reflectance lessens, and the channels are included in the minimization in a linear fashion up to optical depths of 1.50 and 1.00 in bands 1 and 2 respectively, at which point they are fully weighted in the minimization.

Once $\chi^2_{abs}$ has been minimized as described in §3.5.6.2, its absolute value establishes whether the candidate aerosol model provides a good fit to the measurements. Furthermore, additional parameters are used to determine the goodness of fit of the particular aerosol model to the MISR data. These additional parameters are defined as follows, and are calculated using the optical depth determined from the minimization of $\chi^2_{abs}$ (see §3.5.6.2). One is the angular shape normalized to the mean over all available cameras, which emphasizes camera-to-camera geometric differences.

$$\chi^2_{geom}(\tau) = \frac{\sum_{l=1}^{4} w_l \cdot \left[ \sum_{j=1}^{9} w_j \cdot \nu(l,j) \cdot \frac{\left[ \frac{\rho_{MISR}(l,j)}{\rho_{MISR}(l,allcam)} - \frac{\rho_{model}(l,j)}{\rho_{model}(l,allcam)} \right]^2}{\sigma^2_{geom}(l,j)} \right]}{\sum_{l=1}^{4} w_l \cdot \left[ \sum_{j=1}^{9} w_j \cdot \nu(l,j) \right]} \tag{62}$$

where $\rho_{MISR}(l,allcam)$ is the mean over available cameras for each band, and is given by:

$$\rho_{MISR}(l,allcam) = \frac{\sum_{j=1}^{9} w_j \cdot \nu(l,j) \cdot \rho_{MISR}(l,j)}{\sum_{j=1}^{9} w_j \cdot \nu(l,j)} \tag{62a}$$

and where $\sigma_{geom}$ (a dimensionless quantity) is given by:

$$\sigma_{geom}(l,j) = k \cdot \frac{\rho_{MISR}(l,j)}{\rho_{MISR}(l,allcam)} \tag{63}$$

where $k$ is a tunable parameter, ***chisq_uncertainty_multiplier*** in the aerosol science configuration file.

*Equation deleted* (63a)

Another goodness-of-fit parameter is angular shape of the spectral ratio relative to band 3:

$$\chi^2_{spec}(\tau) = \frac{\sum_{\substack{l=1,\\ l\neq 3}}^{4} w_l \cdot \left[ \sum_{j=1}^{9} w_j \cdot \nu''(l,j) \cdot \frac{\left[ \frac{\rho_{MISR}(l,j)}{\rho_{MISR}(band3,j)} - \frac{\rho_{model}(l,j)}{\rho_{model}(band3,j)} \right]^2}{\sigma^2_{spec}(l,j)} \right]}{\sum_{\substack{l=1,\\ l\neq 3}}^{4} w_l \cdot \left[ \sum_{j=1}^{9} w_j \cdot \nu''(l,j) \right]} \tag{64}$$

where $\nu''(l,j) = 1$ if valid values of $\rho_{MISR}(l,j)$ and $\rho_{MISR}(band3,j)$ exist; otherwise $\nu''(l,j) = 0$. For dark water, the summation over $l$ in Eq. (64) includes only band 4. We also have that

$$\sigma_{spec}(l,j) = k \cdot \frac{\rho_{MISR}(l,j)}{\rho_{MISR}(band3,j)} \tag{65}$$

*Equation deleted* (65a)

where $k$ is a tunable parameter, ***chisq_uncertainty_multiplier*** in the aerosol science configuration file.

The advantage of defining metrics such as those given in Eqs. (62) and (64) is that the instrument relative accuracies are higher than the absolute accuracy, thus providing potentially greater sensitivity. Simulations have shown that $\chi^2_{geom}$ tends to be more sensitive to particle size than to composition, whereas $\chi^2_{abs}$ tends to depend more on both particle size and composition.

We also define a maximum deviation parameter:

$$\chi^2_{maxdev}(\tau) = \underset{l,j}{Max} \left\{ w_l \cdot \left[ \frac{\left[ \rho_{MISR}(l,j) - \rho_{model}(l,j) \right]^2}{\sigma^2_{abs}(l,j)} \right] \right\} \tag{66}$$

to find the channel at which the observed equivalent reflectance is most different from the model equivalent reflectance.

Successful aerosol models are those for which all four metrics, $\chi^2_{abs}$, $\chi^2_{geom}$, $\chi^2_{spec}$, and $\chi^2_{maxdev}$, are ≤ threshold values (***max_chisq_abs_dw_thresh, max_chisq_geom_dw_thresh, max_chisq_spec_dw_thresh,*** and ***max_chisq_maxdev_dw_thresh*** in the aerosol science configuration file). These thresholds may be adjusted pending further theoretical sensitivity studies and experience with actual MISR data. Currently, the thresholds are set to 2, 3, 3, and 5 respectively.

Additional constraints on the successful aerosol models are applied, to guard against blunders. First, the retrieved optical depth for a model must be ≤ the product of the optical depth

upper bound for that model and a configurable parameter, ***abs_tau_upperbnd_fraction*** in the aerosol science configuration file. Second, the optical depth uncertainty for a model must be ≤ a configurable parameter, ***max_tau_unc_abs_thresh***, in the aerosol science configuration file. These parameters are currently set to 0.99 and 0.1 respectively.

An additional residual, ζ, know as the combined residual, is computed to determine which single aerosol model will be designated as the lowest residual. It combines the $\chi^2$ parameters with the optical depth uncertainty $\tau_{unc}$, defined in Eq. 81, as follows:

$$\zeta = \sqrt{\left(\frac{\chi^2_{abs}}{\left(\chi^2_{abs}\right)_{max\_abs\_thresh}}\right)^2 + \left(\frac{\chi^2_{geom}}{\left(\chi^2_{geom}\right)_{max\_geom\_thresh}}\right)^2 + \left(\frac{\chi^2_{spec}}{\left(\chi^2_{spec}\right)_{max\_spec\_thresh}}\right)^2 + \left(\frac{\chi^2_{maxdev}}{\left(\chi^2_{maxdev}\right)_{max\_maxdev\_thresh}}\right)^2 + \left(\frac{\tau_{unc}}{\left(\tau_{unc}\right)_{max\_abs\_thresh}}\right)^2} \quad (66a)$$

where the $\chi^2$ and optical depth uncertainty thresholds are given by ***max_chisq_abs_dw_thresh***, ***max_chisq_geom_dw_thresh***, ***max_chisq_spec_dw_thresh***, ***max_chisq_maxdev_dw_thresh*** and ***max_tau_unc_abs_thresh*** in the aerosol science configuration file.

The residuals in Eqs. (61), (62), (64) and (66) are archived in the aerosol product for each model as ***ChisqAbs, ChisqGeom, ChisqSpec,*** and ***ChisqMaxdev.*** The residuals in Eqs. (61) and (66a) which correspond to the lowest residual aerosol model are archived in the aerosol product as ***RegLowestResidChisq and RegLowestResidCombinedResidual.*** The lowest residual aerosol model and its equivalent reflectance values in each channel are archived as ***RegLowestResid-Mixture*** and ***RegLowestResidMixtureEqRefl***.

*Equation deleted* (67)

*Equation deleted* (68)

*Equation deleted* (69)

*Equation deleted* (69a)

*Equation deleted* (69b)

#### *3.5.5.2.3 Heterogeneous surface*

The reduced sample equivalent reflectance, $J_{x,y}$, defined by Eq. (20), can be considered to be a linear combination of surface functions, $\rho^{land}_{x,y}$, defined to be the sample-dependent component of the TOA equivalent reflectance, i.e.,

$$\rho^{land}_{x,y}\left(-\mu,\mu_0,\phi-\phi_0\right) = \exp\left(-\tau/\mu\right)\frac{1}{\pi}\int_0^1\int_0^{2\pi} R^{surf}_{x,y}\left(-\mu,\mu',\phi-\phi'\right)\rho^{inc}_{x,y}\left(\mu',\mu_0,\phi'-\phi_0\right)\mu' d\mu' d\phi'$$

$$+\frac{1}{\pi}\int_0^1\int_0^{2\pi}\int_0^1\int_0^{2\pi} T\left(-\mu,\mu'',\phi-\phi''\right)R^{surf}_{x,y}\left(-\mu'',\mu',\phi''-\phi'\right)\rho^{inc}_{x,y}\left(\mu',\mu_0,\phi'-\phi_0\right)\mu' d\mu' d\phi' d\mu'' d\phi'' \quad (70)$$

where $\rho_{x,y}^{inc}$ is the equivalent reflectance corresponding to the radiance incident upon the surface. If a single BRF shape is able to describe the view angle variability of the surface within a region (the individual sample reflectance, however, being variable), then the reduced sample equivalent reflectances are proportional to each other, i.e.,

$$J_{x,y,j} = c' \cdot J_{x',y',j} = c \cdot f_{j,1} \tag{71}$$

In this particular case the scatter matrix has rank 1, producing a single EOF, $f_{j,1}$, which is proportional to $J_{x,y}$. This is a limited form of Eq. (24). If the correct equivalent reflectance corresponding to the atmospheric path radiance, which is the same as the TOA equivalent reflectance for a black surface $\rho^{black}$, is subtracted from the sample-averaged TOA equivalent reflectance, $\langle \rho_{MISR} \rangle$, then the view angle variability of $\langle \rho_{MISR} \rangle$ - $\rho^{black}$ also must be the same as for the EOF, $f_{j,1}$. This criterion of angular shape comparison determines the best estimate of the aerosol optical depth by requiring that it produce the minimum $\chi^2$ between $\langle \rho_{MISR} \rangle$ - $\rho^{black}$ and $f_{j,1}$. This can be written as

$$\chi^2_{hetero}(\tau) = \frac{\sum_{l=1}^{4}\sum_{j=1}^{9} \nu'''(l,j) \cdot \dfrac{\left[\left|\langle \rho_{MISR}(l,j)\rangle - \rho^{black}(l,j)\right| - A_1(l) \cdot f_{j,1}(l)\right]^2}{\sigma^2_{hetero}(l,j)}}{\sum_{l=1}^{4}\sum_{j=1}^{9} \nu'''(l,j)} \tag{72}$$

where the summation is over the nine MISR view angles and four wavelengths, $\nu'''(l,j)$ = 1 if a valid value of $\langle \rho_{MISR} \rangle$ exists; otherwise $\nu'''(l,j)$ = 0. The quantity $A_1$ is varied to minimize the summation result in a least squares sense, and $\sigma^2_{hetero}$ is defined as:

$$\sigma^2_{hetero} = \left\{0.05 \max(\rho_{MISR}, 0.04)\right\}^2 \tag{72a}$$

When a number of different BRF shapes are represented in the region then Eq. (72) is not rigorously satisfied for the various samples *x, y*. However, we note that the various $J_{x,y}$ are made up of different linear combinations of surface functions, $\rho_{x,y}^{land}$, and these $J_{x,y}$ are most efficiently decomposed using EOFs, $f_{j,n}$, according to Eq. (24). Since $\langle \rho_{MISR} \rangle$ - $\rho^{black}$ is also a linear combination of surface functions it also is efficiently decomposed using the same EOFs. Therefore Eq. (72) can be generalized to

$$\chi^2_{het}(\tau) = \frac{\sum_{l=1}^{4}\sum_{j=1}^{9} \nu'''(l,j) \cdot \dfrac{\left[\left|\langle \rho_{MISR}(l,j)\rangle - \rho^{black}(l,j)\right| - \sum_{n=1}^{N(l)} A_n(l) \cdot f_{j,n}(l)\right]^2}{\sigma^2_{het}(l)}}{\sum_{l=1}^{4}\sum_{j=1}^{9} \nu'''(l,j)} \tag{73}$$

where $N(l)$ (the number of eigenvectors used in band $l$) < $N_{cam}(l)$, where $N_{cam}(l)$ is the number of cameras with valid data in wavelength band $l$, and is given by

$$N_{cam}(l) = \sum_{j=1}^{9} v'''(l,j) \tag{73a}$$

The expansion coefficients $A_n$ are obtained by applying the orthonormality condition of Eq. (23) to the bracketed expression in Eq. (73), i.e.,

$$A_n(l) = \left[\sum_{j=1}^{9}\left[\left\langle \rho_{MISR}(l,j)\right\rangle - \rho^{black}(l,j)\right]\right]\cdot f_{j,n}(l) \tag{74}$$

This expression was modified slightly, as given below:

$$A_n(l) = \frac{\left[\sum_{j=1}^{9}\left[\left\langle \rho_{MISR}(l,j)\right\rangle - \rho^{black}(l,j)\right]\right]}{\Delta\rho_{norm}}\cdot f_{j,n}(l) \tag{74a}$$

where $\Delta\rho_{norm}$ represents the normalization to be applied (specified by ***chisq_het_normalize_flag*** in the aerosol science configuration file).

*Equation deleted* (74b)

However, $\Delta\rho_{norm}$ was later set to unity, and the ***chisq_het_normalize_flag*** set to false, making (74a) equal to (74).

The contribution of an individual eigenvector in describing the angular shape of the surface functions of a given scene is determined by the relative size of its eigenvalue [see §3.4.2.2 and Eq. (26)]. Therefore, only those eigenvectors with eigenvalues greater than or equal to a certain size are used in the summation in Eq. (73). The maximum number of usable eigenvectors in wavelength band $l$, $N_{\max}(l)$, is determined by the condition

$$\sum_{n=N_{\min}}^{N_{\max}(l)-1}\lambda_n < (f_n)_{variance\_thresh}\cdot\sum_{n=N_{\min}}^{N_{cam}(l)}\lambda_n \le \sum_{n=N_{miin}}^{N_{\max}(l)}\lambda_n, \tag{75}$$

i.e., ignoring those eigenvectors which contribute less than a fraction [1 minus $(f_n)_{variance\_thresh}$ or ***eigenvector_variance_thresh*** in the aerosol science configuration file] to the angular variability of the image. $N_{\min}$ is the starting index of the eigenvalue to test, and is set to

***first_eigenvalue_for_eofs*** in the aerosol science configuration file. There is also the constraint that $N_{\max}(l)$ must be less than $N_{cam}(l)$, the total number of eigenvectors.

*Equation deleted* (75a)

*Equation deleted* (75b)

For each of the candidate aerosol models, in each band individually, for each optical depth grid point which is valid according to the HDRF shape mask (described in section 3.4.2.1), a $\chi^2$ is then computed for each value of $N(l)$ used in Eq. (73), starting with all $N(l)$ = 1 (the first eigenvector only) and incrementing the number of eigenvectors by unity but not letting the number exceed $N_{\max}(l)$. Varying the model aerosol optical depth, the minimum $\chi^2$ for each combination of $N(l)$ values, denoted $\chi^2_N$, defines an estimate of the optical depth $\tau_N$. The values of $\tau_N$ in each band are then averaged to get $\tau_{per-band\_mean}$, the per-band mean optical depth for that aerosol model. The associated uncertainty $\Delta\tau_{per-band\_mean}$, is the standard deviation of the per-band optical depths.

For each aerosol model being evaluated, the values $\tau_{per-band\_mean}$ and $\Delta\tau_{per-band\_mean}$ are reported as the best-fitting optical depth, if they were successfully computed. Otherwise, the following approach is used to compute the best-fitting optical depth and uncertainty. In all cases, the value of $\chi^2_{het}$ is computed as follows, and used to determine the successful aerosol models in the series of threshold tests described below.

The quantity $\chi^2_{het}$ over all bands is computed for each aerosol model and its $\tau_{per-band\_mean}$, using Eq. (73). The number of different cases established by this procedure is equal to:

$$N_{cases} = \max_{l} \left\{ N_{\max}(l) \right\} \tag{75c}$$

i.e., the largest value of $N_{\max}(l)$ from among the four wavelength bands.

The following constraints are applied to the retrieved optical depth and associated uncertainty for each of the $N_{cases}$, to guard against blunders in the surface retrieval. First, the retrieved optical depth must be greater than zero, but less than or equal to a fraction of the optical depth upper bound, given by ***het_tau_upperbnd_fraction*** in the aerosol science configuration file:

$$0 < \tau_N \le \left\{ \tau_{upper\_bound} \cdot \left( \tau_{upper\_bound} \right)_{fraction} \right\} \tag{75d}$$

Next, the retrieved optical depth must be less than or equal to an optical depth threshold, given by ***max_het_tau_thresh*** in the aerosol science configuration file:

$$\tau_N \le \tau_{\max\_het\_thresh} \tag{75e}$$

Finally, the uncertainty in the retrieved optical depth as calculated in Eq. (81) must be less than or equal to an optical depth uncertainty threshold, given by ***max_accept_tau_unc_per_het_case*** in the aerosol science configuration file:

$$\Delta\tau_N \le \Delta\tau_{\max\_het\_unc\_thresh} \tag{75f}$$

For each aerosol model, the number of different cases meeting these constraints is equal to $N_{cases\_used}$. The reported best-fitting optical depth is then computed from a weighted average of all $N_{cases\_used}$ optical depths:

$$\tau = \frac{\sum_{N=1}^{N_{cases\_used}} \frac{\tau_N}{\chi_N^2}}{\sum_{N=1}^{N_{cases\_used}} \frac{1}{\chi_N^2}} \tag{76}$$

where the weights are the inverses of the $\chi_N^2$. The formal uncertainty $\Delta\tau$ associated with $\tau$ is then expressed as

$$\Delta\tau = \frac{\sqrt{\sum_{N=1}^{N_{cases\_used}} \frac{\Delta\tau_N}{\chi_N^2}}}{\sum_{N=1}^{N_{cases\_used}} \frac{1}{\chi_N^2}} \tag{77}$$

Finally, the effective $\chi^2$ associated with $\tau$ is defined as the weighted average of all of the $\chi_N^2$:

$$\chi_{het}^2 = \frac{N_{cases}}{\sum_{N=1}^{N_{cases}} \frac{1}{\chi_N^2}} \tag{78}$$

We consider successful aerosol models to be those for which the following constraints are met: $\chi_{het}^2 \le \left(\chi_{het}^2\right)_{max\_het\_thresh}$, where $\left(\chi_{het}^2\right)_{max\_het\_thresh}$ is ***max_chisq_het_thresh*** in the aerosol science configuration file; $\chi_{het}^2 \le \left(\chi_{het}^2\right)_{het\_thresh\_factor} \cdot \left(\chi_{het}^2\right)_{min\_over\_all\_aerosol\_models}$, where $\left(\chi_{het}^2\right)_{het\_thresh\_factor}$ is ***het_chisq_thresh_factor*** and $\left(\chi_{het}^2\right)_{min\_over\_all\_aerosol\_models}$ is the smallest value of $\chi_{het}^2$ out of all aerosol models which also meets the criterion that its optical depth uncertainty is less than ***max_tau_unc_het_thresh***; and $\Delta\tau \le \left(\Delta\tau\right)_{max\_het\_thresh}$ is given by ***max_tau_unc_het_thresh***.

An additional residual is computed, $\zeta$, to determine which single aerosol model will be

designated as the lowest residual. It combines the $\chi^2_{het}$ parameter with the optical depth uncertainty $\chi^2_{unc}$, defined in Eq. 81, as follows:

$$\zeta = \sqrt{\left(\frac{\chi^2_{het}}{\left(\chi^2_{het}\right)_{max\_het\_thresh}}\right)^2 + \left(\frac{\tau_{unc}}{\left(\tau_{unc}\right)_{max\_het\_thresh}}\right)^2} \tag{78a}$$

where $(\tau_{unc})_{max\_het\_thresh}$ is given by ***max_tau_unc_het_thresh*** in the aerosol science configuration file.

The residual in Eq. (73) is archived in the aerosol product for each model as ***ChisqHet.*** The residuals in Eqs. (73) and (78a) which correspond to the lowest residual aerosol model are archived in the aerosol product as ***RegLowestResidChisq*** and ***RegLowestResidCombined-Residual***, and the lowest residual aerosol model and its equivalent reflectance values in each channel are archived as ***RegLowestResidMixture*** and ***RegLowestResidMixtureEqRefl***. The maximum number of usable eigenvectors defined in Eq. (75), $N_{\max(l)}$, is archived as ***NumEofUsed***, and the number of eigenvector cases used in Eqs. (76), (77) and (78), $N_{cases\_used}$, is archived as ***NumAcceptHetOptDepth***. In addition, per-band residuals and optical depths are computed and archived as ***ChisqHetCalcPerBand*** and ***OptDepthHetCalcPer Band***.

### 3.5.6 Compute aerosol optical depth and uncertainty

#### 3.5.6.1 Physics of the problem

Given the methodology for defining residuals as a function of optical depth for each aerosol model, the best-fitting value of $\tau$ for that model is the one which minimizes the appropriate $\chi^2$, i.e., $\chi^2_{abs}$ for the dark water case, and $\chi^2_{het}$ for the heterogeneous land case. Because of the nonlinear dependence on optical depth inherent in the retrievals, there is no analytic method of minimizing the residuals. Instead, the brute force method of stepping through optical depth on a grid is used, starting from the maximum value determined as described in §3.5.4 and working downwards. The result of this process is a tabulated set of $\chi^2$ values as a function of $\tau$. This curve is then used to determine a best-fitting $\tau$ and its associated formal uncertainty.

For the heterogeneous land case, the procedure described in §3.5.5.2.3 is followed.

For the dark water case, additional constraints are placed on the best-fitting $\tau$. First, the retrieved $\tau$ must lie within a certain fraction, ***abs_tau_upperbnd_fraction***, of the optical depth upper bound. Second, the retrieved $\tau$ uncertainty must be less than or equal to a threshold value, ***max_tau_unc_abs_thresh***. If either constraint is not met, then the retrieved $\tau$ for that mixture is not considered successful.

#### 3.5.6.2 Mathematical description of the algorithm

The following steps are used for the dark water case. Given numerical values of $\chi^2$ as a function of $\tau$, the smallest $\chi^2$ and the values on either side of it are used to compute a parabolic fit, represented by the coefficients of the equation

$$\ln\left(\chi^2\right) = A + B\tau + C\tau^2 \tag{79}$$

determined from the three values of $\chi^2$ vs. $\tau$. The logarithm of $\chi^2$ is used instead of $\chi^2$ to guarantee that the minimum value of $\chi^2$, determined from the fitting procedure, is always positive. Then, the optical depth which minimizes $\chi^2$ is given by

$$\tau = -\frac{B}{2C} \tag{80}$$

and the uncertainty in $\tau$ is given by

$$\Delta\tau = \sqrt{\frac{\ln\left(1 + \frac{1}{\chi^2_{min}}\right)}{C}} \tag{81}$$

where $\chi^2_{\min}$ is the minimum $\chi^2$ at $\tau$.

For the heterogeneous land case, if a per-band mean was successfully computed, the optical depth is given by

$$\tau = \frac{\sum_{\lambda} \tau_{\lambda}}{N_{\lambda}} \tag{81a}$$

and the uncertainty in  is given by

$$\Delta\tau = \sqrt{\frac{\sum_{\lambda} \left(\tau_{\lambda} - \tau\right)^2}{N_{\lambda} - 1}} \tag{81b}$$

If a per-band mean was not successfully computed, the optical depth and uncertainty are de fined by Eqs. (76) and (77).

For dark water retrievals, the $\chi^2$ that are reported correspond to the value of $\tau$ determined from Eq. (80), using Eq. (61). In the case of heterogeneous land, the $\chi^2$ that is reported

corresponds to Eq. (78). In the event that the value of $\tau$ which minimizes $\chi^2$ is either of the endpoints (i.e., zero or the upper bound), the aerosol optical depth is set to this value and the formal uncertainty is set to a default value that flags this situation and no formal uncertainty is calculated using Eq. (81). This default value of $\Delta\tau$ is 3.0 (***sigma_tau_default*** in the aerosol science configuration file). In the heterogeneous land situation, where multiple estimates of $\tau$ are combined together, the use of this default value for $\Delta\tau$ causes these cases to be ignored in the weighting procedure. The best-fitting aerosol optical depths for each aerosol model and their associated uncertainties are archived as ***OptDepthPerMixture*** and ***OptDepthUncPer Mixture***.

### 3.5.7 Establish optical depth defaults

#### 3.5.7.1 Physics of the problem

We desire to maximize the coverage of land surface retrievals. These retrievals require at least one regional optical depth value and its associated model. If land aerosol processing fails to find a suitable aerosol model that meets the criteria for a successful retrieval, a default aerosol mod el is established, and a default optical depth is assigned to this model. The default model is chosen from the available Mixture File, and selected to be a model that is believed to represent a "typical" aerosol for land.

#### 3.5.7.2 Mathematical description of the algorithm

The default aerosol model is chosen as the model with the minimum combined residual $\zeta$, defined by Eq. (78a). The default model is not required to be a successful model, as long as the optical depth upper bound for the model is less than a given threshold. If the optical depth upper bound condition is not met for the best fit model in the current region, then it is chosen from a previously processed neighboring region, according to the following hierarchy:

**Error!**

| | | |
|---|---|---|
| 3 | 2 | 5 |
| 1 | X | |
| 4 | | |

As shown in the figure, X represents the current region. The first-choice neighboring region is the region to the left (west) of X. A neighboring region must have at least one successful model for it to be a suitable candidate for choosing a default model, though the default model selected may not be one of the successful models. A neighboring region must also satisfy the optical depth upper bound condition. If the first-choice neighboring region does not provide a suitable default model, then the second-choice neighboring region, the region above (north) of X, is checked. This process continues, until a lowest residual model is found from a neighboring region, or until all five neighboring regions have been checked. Note that the neighboring

regions to the right (east) and below (south) of the current region are not checked, since they have not yet been processed. If no lowest residual model is found, then there is no optical depth default for this region.

The default aerosol model having been specified, the assigned optical depth is established by choosing among the following alternatives.

#### *3.5.7.2.1 Low optical depth upper bound*

If the optical depth upper bound associated with the lowest residual model (see §3.5.4) is ≤ 0.1 in the current region, the default aerosol optical depth is set to:

$$\tau_{default} = \frac{\tau_{upper\_bound}}{2} \tag{81c}$$

In this case the maximum error on the assigned default optical depth is 0.05. The threshold of 0.1 is specified as ***low_tau_default_thresh*** in the aerosol science configuration file.

#### *3.5.7.2.2 Rayleigh only*

This option is no longer used.

#### *3.5.7.2.3 Previous region*

If a previously processed region has a lowest residual optical depth associated with it, and the low optical depth upper bound criterion is not met in the current region, the default aerosol optical depth is set to:

$$\tau_{default} = \tau_{previous\_region\_lowest\_residual} \tag{81d}$$

This default requires that the previous region lowest residual optical depth does not exceed a fraction of the optical depth upper bound for the default aerosol model within the region currently being processed, where the fraction is the product of the optical depth upper bound for the default aerosol model within the region and ***prev_region_default_thresh*** in the aerosol science configuration file, currently set to 0.95.

#### *3.5.7.2.4 Previous region test with upper bound override*

If a previously processed region has a best fit optical depth associated with it, the low optical depth upper bound criterion is not met for the current region, and the previous region test described in §3.5.7.2.3 is not met, the default aerosol optical depth is set to

$$\tau_{default} = \tau_{upper\_bound} \cdot T_{previous\_region\_defauult\_thresh} \tag{81e}$$

where $T_{previous\_region\_defauult\_thresh}$ is specified by ***prev_region_default_thresh*** in the aerosol science configuration file.

The optical depth defaults are archived in the aerosol product as ***RegSfcRetrOptDepth***, ***RegSfcRetrOptDepthUnc, RegSfcRetrMixture*** and ***RegSfcRetrAlgTypeFlag***.

### 3.5.8 Calculate overall regional aerosol optical depth

#### 3.5.8.1 Physics of the problem

The radiometric performance of the instrument will dictate which aerosol models fit the data to within the instrumental uncertainties. Any model fit which meets the criteria described in §3.5.5.2 is deemed to be a valid fit. Of course, the best situation is that only one of the multiple initial guesses will qualify as a best fit. However, it is possible for more than one model to satisfy the goodness-of-fit criteria. Resolution of the ambiguous nature of this situation will require reference to additional information. Finally, it is possible that no model will qualify as fitting the observational data to within the radiometric performance of the instrument. This will be indicative of a failure of the pre-determined models to represent the ambient atmospheric state or some other limitation of the algorithm or instrument performance. Reporting the residual of the fits in the Aerosol/ Surface Product will enable flagging these cases. Experience with actual MISR data will be necessary to determine the needed model improvements. An overall Aerosol Retrieval Success Indicator (**AerRetrSuccFlag** in the aerosol product) is established for each region as a simple way of determining (e.g., for subsequent surface retrieval processing) if at least one good fitting model has been found (see *[M-17]*). A per-model Aerosol Retrieval Success Indicator (**AerRetrSuccFlagPerMixture** in the aerosol product) is also established for each region as a simple way of determining if an individual model has a good fit with the observational data.

Assuming that at least one model meets the goodness-of-fit criteria, and each of these models has an optical depth associated with it as determined according to the algorithm described in §3.5.6, several overall best estimates of aerosol optical depth are calculated, along with measures of the spread in values. Additionally, a single overall best estimate is provided, which is derived from the various overall best estimates. When a default optical depth and its single associated model have been established, all of the best-estimate values correspond to this default.

#### 3.5.8.2 Mathematical description of the algorithm

Given a set of $m$ models that satisfy the goodness-of-fit criteria, where $1 \le m \le$ the total number of models, and the associated optical depths $\tau_m$ for each of these models, the regional estimates of optical depth are given by

$$\begin{aligned} \textbf{\textit{RegMeanSpectralOptDepth}} &= Mean\left(t_m\right) \\ \textbf{\textit{RegMedianSpectralOptDepth}} &= Median\left(t_m\right) \\ \textbf{\textit{RegLowestResidSpectralOptDepth}} &= \tilde{t}_m \end{aligned} \tag{82}$$

The quantity $\tilde{\boldsymbol{t}}_{\boldsymbol{m}}$ is the optical depth for which $\varsigma$ is smallest.

A single best estimate of optical depth, ***RegBestEstimateSpectralOptDepth***, is also reported. This overall best estimate is derived from the mean. At regions where no retrieval is attempted or no successful models are found, a 3x3 (52.8 km x 52.8 km) average of surrounding regions may be calculated to fill in the best estimate optical depth for the missing retrieval. For a 3x3 average to be calculated, there must be at least 5 (configurable parameter ***best_est_3x3_min_-succ_retr***) neighboring regions with successful retrievals.

Variation is also calculated:

$$\sigma = Standard\ deviation\left(t_m\right) \tag{82a}$$

and stored in the product as ***RegStDevSpectralOptDepth.***

The overall best estimate of optical depth uncertainty, ***RegBestEstimateSpectralOpt-DepthUnc***, is set to σ when more than one model satisfied the goodness-of-fit criteria. If only one model satisfied the goodness-of-fit criteria, it is set to the uncertainty for that model. If no models satisfy the goodness-of-fit criteria, the fields are flagged with fill values.

The quality flag ***RegBestEstimateQA*** indicates how the single optical depth best estimate was computed. This flag is set to

- 0 if there is a single successful mixture
- 1 if there are more than 1 successful mixtures
- 2 if the 3x3 surrounding subregions are used to fill in the missing retrieval data

A quality flag indicating the success of the aerosol retrieval is archived as ***AerRetrSuccFlag***. Additionally, the mean and median are calculated and reported over each 70.4 km x 70.4 km domain and archived as ***DomMeanOptDepth*** and ***DomMedOptDepth***. Furthermore, a two-dimensional histogram of the regional $\tau_n$ values within a domain is provided, ***OptDepthHistogram***, where one dimension is aerosol mixture and the other is optical depth in steps of 0.05.

### 3.5.9 Compute Angstrom exponent

#### 3.5.9.1 Physics of the problem

The Angstrom exponent is computed from the regional best estimate optical depths. The Angstrom exponent can be used as a proxy for aerosol particle size.

#### 3.5.9.2 Mathematical description of the algorithm

A least-squares straight line fit is computed from the natural logarithm of the best estimate aerosol optical depths as a function of the natural logarithm of wavelength at all four MISR wavelengths. The Angstrom exponent is the negative of the slope of the fitted line. The

resulting Angstrom exponent and uncertainty are stored in the product as ***RegBestEstimate-AngstromExponent*** and ***RegBestEstimateAngstromExponentUnc***.

### 3.5.10 Calculate remaining aerosol particle properties

#### 3.5.10.1 Physics of the problem

Properties such as size, shape, and brightness vary among aerosol types. MISR sensitivities to these properties enable us to distinguish these properties among aerosol types. Particle sizes are distinguishable into broad groups of small, medium and large particles, and particle shape into spherical vs. non-spherical groupings. Brightness is expressed in terms of single-scattering albedo. For the aerosol model with the lowest residual and which meets the goodness-of-fit criteria, several aerosol properties are calculated, along with measures of the spread in values.

#### 3.5.10.2 Mathematical description of the algorithm

Several properties of the aerosol mixtures which satisfy the goodness-of-fit criteria are determined. For each mixture, the fraction of particles which are small, medium, and large, where small particles are those with radii < 0.35 μm, medium are those with radii in the range 0.35 to 0.7 μm, and large particles are those with radii > 0.7 μm, are computed by number fraction, volume fraction, and optical depth fraction, and stored in the ACP, as described in Section 3.5.11 of *[M-11]* (Rev. C.). The fraction of particles which are spherical and non-spherical are also reported in the ACP, as described in Section 3.5.11 of *[M-11]* (Rev. C). Single-scattering albedo for the aerosol mixtures is reported in the ACP; see Section 3.5.10 of *[M-11]*.

The mean optical depth for each class of small, medium, large, spherical, and non-spherical particles is calculated as

$$\bar{\tau}_{class}(\lambda) = \frac{1}{N_{mixture}} \sum_{mixture} f_{class}(\boldsymbol{mixture}, \lambda) \cdot \tau(\boldsymbol{mixture}, \lambda) \tag{83}$$

where $\lambda$ is spectral band, $f_{class}(\boldsymbol{mixture}, \lambda)$ is the fraction of optical depth belonging to the class for each successful mixture and spectral band, $\tau(\boldsymbol{mixture}, \lambda)$ is the total optical depth for the mixture and spectral band, and $N_{mixture}$ is the total number of successful mixtures.

Total mean optical depth is

$$\bar{\tau}(\lambda) = \frac{1}{N_{mixture}} \sum_{mixture} \tau(\boldsymbol{mixture}, \lambda) \tag{84}$$

The fraction of mean optical depth in each class is then

$$\overline{f}_{class}(\lambda) = \frac{\overline{\tau}_{class}(\lambda)}{\overline{\tau}(\lambda)} = \frac{\sum_{mixture} f_{class}(\boldsymbol{mixture}, \lambda) \cdot \tau(\boldsymbol{mixture}, \lambda)}{\sum_{mixture} \tau(\boldsymbol{mixture}, \lambda)} \tag{86}$$

Note that

$$\bar{f}(\lambda) = \bar{f}_{small}(\lambda) + \bar{f}_{medium}(\lambda) + \bar{f}_{large}(\lambda)$$

$$= \bar{f}_{spherical}(\lambda) + \bar{f}_{non-spherical}(\lambda) \tag{85}$$

The uncertainty in optical depth for each class is computed as

$$\sigma_{\tau, class}(\lambda) = \sqrt{\frac{1}{N_{mixture}} \sum_{mixture} \left[ f_{class}(\boldsymbol{mixture}, \lambda) \cdot \tau(\boldsymbol{mixture}, \lambda) - \overline{\tau}_{class}(\lambda) \right]^2} \tag{88}$$

The uncertainty in fraction for each class is

$$\sigma_{f, class}(\lambda) = \frac{\sigma_{\tau, class}(\lambda)}{\overline{\tau}_{class}(\lambda)} \tag{89}$$

The fractions at the lowest residual mixture for each class at each spectral band are also computed:

$$f_{lr, class}(\lambda) = \frac{\tau_{lr, class}(\lambda)}{\tau_{lr}(\lambda)} \tag{87}$$

where $\tau_{lr}(\lambda)$ is the optical depth for the lowest residual mixture at band $\lambda$ and $\tau_{lr, class}(\lambda)$ is the optical depth due to the *class* of particles at band $\lambda$ for the lowest residual mixture.

The quantities are reported in the aerosol product as ***RegMeanSpectralOptDepth-Fraction, RegStDevSpectralOptDepthFraction and RegLowestResidSpectralOptDepth-Fraction.*** The size fraction information and shape fraction information have been combined into the same fields, for simplicity. Single-scattering albedo, number fraction, and volume fraction are computed and reported as ***RegMeanSpectralSSA, RegStDevSpectralSSA, RegLowestResid-SpectralSSA, RegLowestResidNumberFraction,*** and ***RegLowestResidVolumeFraction.***

A single overall best estimate of each aerosol property is also reported, using the lowest residual mixture. The best estimates are reported as ***RegBestEstimateSpectralOptDepth-Fraction, RegBestEstimateSpectralOptDepthFractionUnc, RegBestEstimateSpectralSSA, RegBest-EstimateNumberFraction, RegBestEstimateVolumeFraction***.

Particle properties should only be used when the best estimate optical depth is above a configurable threshold, ***pprop_opt_depth_qa_thresh***, currently set to 0.15. The region flag

***RegParticle-PropertyQA*** is set to 1 to reflect this condition in the aerosol product.

## 3.6 PRACTICAL CONSIDERATIONS

### 3.6.1 Numerical computation considerations

Requirements on processing speed and data storage are described in *[M-16]*.

### 3.6.2 Configuration of retrievals

An Aerosol Retrieval Configuration File is used to establish the numerical values of adjustable parameters used within the retrievals, e.g., thresholds establishing whether a successful retrieval occurred. This avoids "hard-wiring" specific values into the software. The Aerosol/Surface Product will contain information indicating what version of the configuration file was used. The contents of the Aerosol Retrieval Configuration File are shown in Table 6. The values shown correspond to the settings at the time this document was generated (AS_SCI_CONFIG version F12_0020); however, the annotation text of the Level 2 Aerosol Product should be checked to determine the actual threshold values used in the retrievals. The italicized name in parentheses after the parameter description is the name of the parameter in the annotation text. The column entitled "Section" indicates where in this ATB a description of the specific configuration parameter is found.

**Table 5: Contents of the Aerosol Retrieval Configuration File**

| Parameter | Value | Section |
|---|---|---|
| Regional cosine of solar zenith angle (**SolZenAng**) threshold *(mu0_thresh)* | 0.2 | 3.3.1.2.1 |
| Regional topographic complexity threshold *(region_topo_complex_thresh)* | 500 m | 3.3.1.2.2 |
| Regional cloudiness threshold (high confidence cloud fraction) *(hc_cloud_pcnt_thresh)* - OBSOLETE. THIS TEST IS NO LONGER USED | 100% | 3.3.1.2.3 |
| Regional cloudiness threshold (low confidence cloud fraction) *(lc_cloud_pcnt_thresh)* - OBSOLETE. THIS TEST IS NO LONGER USED | 100% | 3.3.1.2.3 |
| Maximum acceptable RDQI used in averaging data to appropriate resolution, $RDQI_1$ *(rdqi1)* | 1 | 3.3.2.2 |
| $RDQI_2$ [value of RDQI' in Eq. (3a) if RDQI > $RDQI_1$] *(rdqi2)* | 3 | 3.3.2.2 |
| Subregional topographic complexity threshold *(subr_topo_complex_thresh)* | 250 m | 3.3.8.2.5 |
| Maximum allowable subregion average slope *(max_subr_avg_slope)* | 20° | 3.3.8.2.5 |
| Particle property QA is set to "bad" if green band optical depth is less than this threshold. (*pprop_opt_depth_qa_thresh*) | 0.15 | 3.5.10.2 |
| Cloud mask decision logic *(cloud_mask_decision_matrix)* | See Table 5 | 3.3.8.2.6 |
| Maximum acceptable RDQI for inclusion in retrieval, $RDQI_3$ *(rdqi3)* | 0 | 3.3.8.2.8 |
| Brightness threshold (*bright_thresh*) for snow/ice, water, and land, | 1.0, 0.5, 0.5 | 3.3.8.2.9 |

| | | |
|---|---|---|
| respectively | | |
| Minimum scattering angle considered to be rainbow-influenced *(min_rainbow_omega, min_rainbow_dw_omega)* | 110°, 110° | 3.3.8.2.10 |
| Maximum scattering angle considered to be rainbow-influenced *(max_rainbow_omega, max_rainbow_dw_omega)* | 160°, 160° | 3.3.8.2.10 |
| Threshold for $\chi^2_{smooth}$ *(chisq_smooth_thresh)* | 4 | 3.3.8.2.10 |
| Maximum acceptable RDQI for inclusion in angle-to-angle correlation test, $RDQI_4$ *(rdqi4)* | 1 | 3.3.8.2.11 |
| Correlation mask variance limit *(corr_mask_variance_limit)* | 1.0E-06 | 3.3.8.2.11 |
| Regional correlation mask variance limit *(reg_corr_mask_variance_limit)* | 1.0E-08 | 3.4.2.2 |
| Angle-to-angle correlation threshold *C*thresh *(ang_corr_thresh)* | 0.25 | 3.3.8.2.11 |
| Regional angle-to-angle correlation threshold *(reg_ang_corr_thresh)* | 0.10 | 3.4.2.2 |
| Albedo threshold used in constraining optical depth upper bound over land *(albedo_thresh_land)* | 0.015 | 3.5.4 |
| Albedo threshold used in constraining optical depth upper bound over water *(albedo_thresh_water)* | 0.0 | 3.5.4 |
| If true, use the max scaled optical depth value over channel for land pixels to determine OD upper bound; otherwise use the min (*land_maxval_flag*) | false | 3.5.4.2 |
| If true, use the max scaled optical depth value over channel for water pixels to determine OD upper bound; otherwise use the min (*water_maxval_flag*) | true | 3.5.4.2 |
| Default value for optical depth uncertainty when parabolic fit in Eq. 81 can not be computed *(sigma_tau_default)* | 3.0 | 3.5.6.2 |
| Minimum number of usable subregions in a region required to designate channel as Dark Water *(min_dw_subr_thresh)* | 32 | 3.4.5.2 |
| Minimum number of usable cameras in a subregion for dark water retrievals, *(min_dw_cam_thresh)* | 4 | 3.4.5.2 |
| Identifies spectral bands to use in dark water retrievals. Dimensioned by the 4 spectral bands. *(dw_band_mask)* | (true,true,true,true) | 3.4.5.2 |
| Maximum value of $\chi^2_{abs}$ (**ChisqAbs**) for successful dark water retrieval *(max_chisq_abs_dw_thresh)* | 2 | 3.5.5.2.1 |
| Maximum value of $\chi^2_{geom}$ (**ChisqGeom**) for successful dark water retrieval *(max_chisq_geom_dw_thresh)* | 3 | 3.5.5.2.1 |
| Maximum value of $\chi^2_{spec}$(**ChisqSpec**) for successful dark water retrieval *(max_chisq_spec_dw_thresh)* | 3 | 3.5.5.2.1 |
| Maximum value of $\chi^2_{maxdev}$ (**ChisqMaxdev**) for successful dark water retrieval *(max_chisq_maxdev_dw_thresh)* | 5 | 3.5.5.2.1 |
| Fraction of optical depth upper bound (**OptDepthUpBd**) above which optical depth values are eliminated *(abs_tau_upperbnd_fraction)* | 0.99 | 3.5.5.2.1, 3.5.6.1 |

| | | |
|---|---|---|
| Maximum allowable value of optical depth uncertainty for successful dark water retrieval *(max_tau_unc_abs_thresh)* | 0.1 | 3.5.5.2.1, 3.5.6.1 |
| Per-band value used to establish optical depth weighting factor controlling which optical depth grid points are used in dark water retrieval, down to a minimum optical depth grid point (*dw_tau_min_for_weights*) | 0.75, 0.50, 0.00, 0.00 | 3.5.5.2.1 |
| Per-band value used to establish optical depth weighting factor controlling which optical depth grid points are used in dark water retrieval, up to a maximum optical depth grid point (*dw_tau_max_for_weights*) | 1.50, 1.00, 0.00, 0.00 | 3.5.5.2.1 |
| Tunable multiplier used in calculating sigma_geom and sigma_spec *(chisq_uncertainty_multiplier)* | 0.05 | 3.5.5.2.1 |
| Minimum number of common subregions required to perform aerosol retrieval over heterogeneous surfaces *(min_het_subr_thresh)* | 16 | 3.4.2.2 |
| Minimum standard deviation of equivalent reflectance required by the aerosol algorithm over heterogeneous surfaces *(min_het_stdev_thresh)* - OBSOLETE. THIS TEST IS NO LONGER USED | 0.0 | - |
| Band to use for screening common subregions by weighted mean radiance in aerosol retrieval over heterogeneous surfaces *(het_filter_band)* | 3 | 3.4.2.2 |
| Threshold for radiances used in contrast algorithm for aerosol algorithm over heterogeneous surfaces *(het_land_radiance_thresh)* | 1.0 | 3.4.2.2 |
| Bands used by aerosol algorithm over heterogeneous surfaces. *(het_band_mask)* | true, true, true, true | 3.4.2.2 |
| Maximum value of $\chi^2_{het}$ (**ChisqHet**) for successful aerosol retrieval over heterogeneous surfaces *(max_chisq_het_thresh)* | 4.0 | 3.5.5.2.3 |
| Configurable factor multiplied by minimum $\chi^2_{het}$ (**ChisqHet**) across all successful mixtures used to constrain which mixtures succeed in aerosol retrievals over heterogeneous surfaces *(het_chisq_thresh_factor)* | 1.5 | 3.5.5.2.3 |
| Maximum allowable value of optical depth uncertainty for successful aerosol retrieval over heterogeneous surfaces *(max_tau_unc_het_thresh)* | 0.1 | 3.5.5.2.3 |
| Those eigenvalues which account for at least this fraction of the variance in the scene are used for expansion coefficients (*eigenvector_variance_thresh*) | 0.99 | 3.5.5.2.3 |
| Starting index of eigenvalue to test in computing number of eigenvalues to use for expansion coefficients *(first_eigenvalue_for_eofs)* | 2 | 3.5.5.2.3 |
| Fraction of optical depth upper bound above which optical depth values are eliminated in aerosol retrieval over heterogeneous surfaces *(het_tau_upperbnd_fraction)* | 0.99 | 3.5.5.2.3 |
| Maximum value of acceptable optical depth for aerosol retrieval over heterogeneous surfaces *(max_het_tau_thresh)* | 3.0 | 3.5.5.2.3 |
| Maximum value of acceptable optical depth uncertainty for individual cases in aerosol retrieval over heterogeneous surfaces | 3.0 | 3.5.5.2.3 |

| | | |
|---|---|---|
| (*max_accept_tau_unc_per_het_case*) | | |
| Threshold for optical depth upper bound below which the low optical depth default is used *(low_tau_default_thresh)* | 0.1 | 3.5.7.2.1 |
| Threshold for default optical depth below which the previous region optical depth default is used *(prev_region_default_thresh)* | 0.95 | 3.5.7.2.3 |
| Flag indicating whether to normalize (rho_misr - rho_model) by its camera average *(chisq_het_normalize_flag)* | false | 3.5.5.2.3 |
| Flag which sets aerosol algorithm type to aerosol retrieval over homogeneous surfaces if the aerosol algorithm over heterogeneous surfaces is not suitable *(do_homog_retrieval)* - THIS ALGORITHM IS NOT USED OPERATIONALLY. IT IS UNDERGOING EVALUATION. | false | - |
| Logical mask specifying which bands to use to compute the homogeneous chi-square residual *(homog_band_mask)* | true, true, true, true | 3.4.2.2 |
| Minimum number of cameras required by the aerosol algorithm over homogeneous surfaces *(homog_min_cam_thresh)* - NOT USED. THIS ALGORITHM IS CURRENTLY TURNED OFF. | 6 | - |
| Minimum number of subregion locations required by the aerosol algorithm over homogeneous surfaces *(homog_min_subr_thresh)* - NOT USED. THIS ALGORITHM IS CURRENTLY TURNED OFF. | 8 | - |
| Maximum value of chi-square residual for successful aerosol retrieval over homogeneous surface *(max_chisq_homog_thresh)* | 10.0 | 3.4.2.2 |
| Number of optical depth grid points to extend the Hdrf_shape_tau_mask tau window if numtau = 1 *(num_tau_extra)* | 2 | 3.4.2.2 |
| Flag which determines whether to apply camera-specific weights emphasizing oblique angle *(cam_weight_oblique_flag)* | true | 3.4.2.2 |
| Flag which determines whether to apply camera-specific weights emphasizing near-nadir angle *(cam_weight_nadir_flag)* | false | 3.4.2.2 |
| Flag which determines whether to apply band-specific weights emphasizing short wavelengths *(band_weight_short_flag)* | true | 3.4.2.2 |
| Flag which determines whether to apply band-specific weights emphasizing long wavelengths *(band_weight_long_flag)* | false | 3.4.2.2 |
| Fraction of optical depth upper bound above which optical depth values are eliminated in aerosol retrieval over homogeneous surface *(homog_tau_upperbnd_fraction)* - NOT USED. THIS ALGORITHM IS CURRENTLY TURNED OFF. | 0.99 | 3.4.2.2 |
| Maximum allowable value of optical depth uncertainty for successful aerosol retrieval over homogeneous surface *(max_tau_unc_homog_thresh)* | 0.1 | 3.4.2.2 |
| Weight given to angular and spectral methods in constraining the mixtures in the Hdrf_shape_tau_mask *(frac_geom_spec_mix)* | 0.5 | 3.4.2.2 |

| | | |
|---|---|---|
| Weight given to angular and spectral methods in constraining the optical depths in the Hdrf_shape_tau_mask *(frac_geom_spec_tau)* | 0.5 | 3.4.2.2 |
| Number of points in smoothing filter used for heterogeneous and homogeneous optical depth residuals; must be an odd number; 1 = turn off smoothing *(resid_filter_width)* | 1 | 3.4.2.2 |
| Maximum computed number of iterations for hdrf computation in aerosol retrieval over homogeneous surfaces; a value of 0 turns off hdrf iteration (*hdrf_conv_iter_as*) | 0 | 3.4.2.2 |
| Angular shape threshold multiplying factor *(hdrf_thresh_factor_mix)* | 2.0 | 3.4.2.2 |
| Shape threshold multiplying factor for optical depths *(hdrf_thresh_factor_tau)* | 2.0 | 3.4.2.2 |
| Cameras with glitter angles less than this threshold are not used. (*glitter_threshold*) | 40.0 | 3.3.8.2.3 |

### 3.6.3 Quality assessment and diagnostics

A number of parameters and indicators will be reported in the Aerosol/Surface Product as retrieval diagnostics. Maps or other summaries of these parameters will be reviewed by the MISR team for quality assessment. Included among these are retrieval residuals, sources of ancillary and external data, statistical information regarding the processing, etc. A tabulation of these indicators is provided in *[M-17]*, cross-referenced, where applicable, to the pertinent section of this ATB.

### 3.6.4 Exception handling

Exception handling has been discussed as part of each algorithm description.

## 3.7 ALGORITHM VALIDATION

Validation of the aerosol retrieval algorithms will rely on several sources of data including aircraft observations, together with field observations of downwelling diffuse sky spectral radiance and irradiance, the direct solar irradiance component and the surface spectral bidirectional reflectance factor (BRF).

In contrast to MISR or aircraft observations of the upwelling radiation field at the top or middle of the atmosphere, ground-based deployments obtain downwelling measurements of sky spectral diffuse radiance and irradiance together with the directly transmitted solar irradiance. The validation approach adopted for MISR consists of comparing geophysical parameters generated using MISR with independent algorithms on ground-based observations in order to secure ground-based estimates of aerosol spectral optical depth, effective size distribution, phase function, and single scattering albedo. Thus, retrievals will be carried out, where applicable, both by forward calculations with radiative transfer models based on the MISR Aerosol Climatology

Product, and according to formal inversion procedures involving the governing integral equations.

Details on planned field campaigns, experimental methodologies, and instrument calibration and data reduction procedures are documented in *[M-15]*. In addition, *[M-12]* provides the theoretical basis behind the algorithms to be used as part of the validation activity. For this information, the reader is referred to those sources.

# 4. ASSUMPTIONS AND LIMITATIONS

## 4.1 ASSUMPTIONS

The following assumptions are made with respect to the aerosol retrievals described in this document:

(1) Hydrated aerosol particles are modeled as homogeneous spheres.

(2) Medium-mode nonspherical dust particles are modeled as randomly oriented grains, with observationally constrained, size-dependent sphericity (Kalashnikova et al., 2005). Course-mode nonspherical dust particles are modeled as randomly oriented prolate and oblate spheroids with a uniform distribution of aspect ratios between 1.2 and 2.2 (Mishchenko et al., 1997; Kalishnikova et al., 2005). This will likely be changed in the MISR standard retrieval algorithm once the performance of new models, constrained by recent field data (e.g. Dubovik et al., 2006), is analyzed.

(3) Nonspherical thin cirrus particles are modeled as randomly oriented 20 micron hexagonal prisms (Takano and Liou, 1989). This is not yet implemented in the MISR standard retrieval algorithm, pending assessment of alternative cirrus models.

(4) Natural mixtures of atmospheric aerosols are homogeneous, external mixes of pure particles types contained in the ACP.

(5) The aerosol mixtures specified by the ACP span the range of natural conditions for the duration of the EOS mission.

(6) Measurements corresponding to each 17.6 km x 17.6 km region upon which an aerosol retrieval is performed are assumed to be acquired through a locally horizontally homogeneous atmosphere.

(7) MISR bands 1, 2, and 3 are assumed to be unaffected by water vapor in the atmosphere. Water vapor column abundance will be taken into account in MISR band 4 during calculation of the SMART Dataset, using a standard atmospheric profile. The water vapor optical depth in band 4 is small enough that this procedure leads to negligible errors.

(8) Climatological values of ozone column abundance will be used. Corrections for ozone absorption will be made to all MISR channels.

(9) $NO_2$ absorption affects MISR bands 1 and 2. However, over most of the globe, the maximum column optical depth of $NO_2$ is small enough (i.e., $< 0.002$), to be neglected.

## 4.2 LIMITATIONS

The following limitations apply to the at-launch aerosol retrievals described in this docu-

ment:

(1) Retrievals will not be performed when the cosine of the solar zenith angle is less than 0.2.

(2) Retrievals will not be performed over topographically complex terrain.

# 5. REFERENCES


Bevington, P.R. (1969). *Data reduction and error analysis for the physical sciences.* McGraw-Hill, Inc., 336 pp.

d'Almeida, G. A., P. Koepke, and E. P. Shettle (1991). *Atmospheric Aerosols: Global climatology and radiative characteristics.* Deepak Publishing.

Deering, D.W. and P. Leone (1986). A sphere-scanning radiometer for rapid directional measurements of sky and ground radiance. *Rem. Sens. Environ.* **19**, 1-24.

Diner, D. J. and J. V. Martonchik (1985a). Influence of aerosol scattering on atmospheric blurring of surface features. *IEEE Trans. Geosci. and Rem. Sens.* **GE-23**, 618-624.

Diner, D. J. and J. V. Martonchik (1985b). Atmospheric transmittance from spacecraft using multiple view angle imagery. *Appl. Opt.* **24**, 3503-3511.

Diner, D. J., J. V. Martonchik, R. A. Kahn, B. Pinty, N. Gobron, D. L. Nelson, B. N. Holben (2005), Using angular and spectral shape similarity constraints to improve MISR aerosol and surface retrievals over land, *Remote Sensing of Environment*, 155-171.

Diner, D.J., S.R. Paradise, and J.V. Martonchik (1994). Development of an aerosol opacity retrieval algorithm for use with multi-angle land surface images. *Proceedings of the IGARSS'94 Symposium* (Pasadena, CA).

Dubovik, O., et al. (2006). Application of spheroid models to account for aerosol particle nonsphericity in remote sensing of desert dust, J. *Geophys. Res.* 111, doi:1029/2005JD006619.

Engelsen, O., B. D. Pinty, and M. M. Verstraete (1996). Parametric Bidirectional Reflectance Factor (BRF) models: I. Evaluation. Internal report, Institute for Remote Sensing Applications, Joint Research Centre, Ispra, Italy.

Flowerdew, R. J. and J. D. Haigh (1995), An approximation to improve accuracy in the derivation of surface reflectances from multi-look satellite radiometers. *Geophys. Res. Lett.* **22**, 1693-1696.

Fraser, R. S. (1976). Satellite measurement of mass of Sahara dust in the atmosphere. *Appl. Opt.* **15**, 2471-2479.

Gordon, H. R. and D. K. Clark (1981). Clear water radiances for atmospheric correction of Coastal Zone Color Scanner imagery. *Appl. Opt.* **20**, 4175-4180.

Gordon H. R. (1984). Some studies of atmospheric optical variability in relation to CZCS atmospheric correction (NOAA National Environmental Satellite and Data Information Service, Final Report Contract No. NA-79-SAC-00714).

Gordon, H. R. (1994). Presentation to the MISR Science Team, Pasadena, CA, March.

Govaerts, Y. and M. M. Verstraete (1994). Applications of the L-systems to canopy reflectance modelling in a Monte Carlo Ray Tracing technique. In *Multispectral and Microwave Sensing of Forestry, Hydrology, and Natural Resources*, SPIE, Rome.

Grant, I.P. and G.E. Hunt (1968). Solution of radiative transfer problems using the invariant $S_n$ method. *Mon. Not. Roy. Astron. Soc.* **141**, 27-41.

Griggs, M. (1975). Measurements of atmospheric aerosol optical thickness over water using ERTS-1 data. *J. Air Pollut. Control Assoc.* **25**, 622-626.

Griggs, M. (1983). Satellite measurements of tropospheric aerosols. *Adv. Space Res.* **2**, 109.

Hansen, J.E., and L.D. Travis (1974). Light scattering in planetary atmospheres. *Space Sci. Rev.* **16**, 527-610.

Holben, B.N., T.F. Eck, I. Slutsker, D. Tanre, J.P. Buis, A. Setzer, E. Vermote, J.A. Reagan, Y.J. Kaufman, T. Nakajima, F. Lavenu, I. Jankowiak, and A. Smirnov (1998), AERONET A federated instrument network and data archive for aerosol characterization. *Rem. Sens. Environ.* **66**, 1-16.

Irons, J. R., K. J. Ranson, D. L. Williams, R. R. Irish, and F. G. Huegel (1991). An off-nadir-pointing imaging spectroradiometer for terrestrial ecosystem studies. *IEEE. Trans. Geosci. Rem. Sens.* **GE-29**, 66-74.

Kahn, R., R. West, D. McDonald, B. Rheingans, and M.I. Mishchenko (1997). Sensitivity of multi-angle remote sensing observations to aerosol sphericity. *J. Geophys. Res.* **102**, 16,861-16,870

Kalashnikova, O. V., R. Kahn, I. N. Sokolik, and W-H. Li (2005). The ability of multi-angle remote sensing observations to identify and distinguish mineral dust types: Part 1. Optical models and retrievals of optically thick plumes, *J. Geophys. Res.*, doi: 10.1029/2004JD004550.

Kaufman, Y. J., and C. Sendra (1988). Algorithm for atmospheric corrections. *Int. J. Remote Sens*. **9**, 1357-1381.

Kaufman, Y.J. and D.Tanre (1992). Atmospherically Resistant Vegetation Index (ARVI) for EOS-MODIS. *IEEE Trans. Geosci. Rem. Sens.* **30**, 261-270.

Kimes, D. S. (1983). Dynamics of directional reflectance factor distributions for vegetation canopies. *Appl. Opt.* **22**, 1364-1372.

Kimes, D.S., W. Newcomb, C. Tucker, I. Zonneveld, W. van Wijngaarden, J. de Leeuw,

and G. Epema (1985). Directional reflectance factor distributions for cover types of northern Africa in NOAA 7/8 AVHRR bands 1 and 2. *Rem. Sens. Environ.* **18**, 1-19.

Kimes, D. S., W. W. Newcomb, R. F. Nelson, and J. B. Schutt (1986). Directional reflectance distributions of a hardwood and pine forest canopy. *IEEE Trans. Geosci. Rem. Sens.* **GE-24**, 281-293.

Kimes, D.S. and W.W. Newcomb (1987). Directional scattering properties of a wintering deciduous hardwood canopy. *IEEE Trans. Geosci. Rem. Sens.* **25**, 510-515.

King, M. D., Y. J. Kaufman, W. P. Menzel, and D. Tanre (1992). Remote sensing of cloud, aerosol, and water vapor properties from the Moderate resolution Imaging Spectrometer (MODIS). *IEEE Trans. Geosci. Remote Sens.* **30**, 2-27.

Krekov, G. M. (1993). Models of atmospheric aerosols, in *Aerosol Effects on Climate*, S. G. Jennings, ed., University of Arizona Press, 304 pp.

Long, C. S., and L. L. Stowe (1993). Using the NOAA/AVHRR to study stratospheric aerosol optical thickness following the Mt. Pinatubo eruption. *Geophys. Res. Lett*., submitted.

Mackay, G., M.D. Stevens, and J.A. Clark (1998). An atmospheric correction procedure for the ATSR-2 visible and near-infrared land surface data. *Int. J. Remote Sensing* **19**, 2949-2968.

Martonchik, J. V., and D. J. Diner (1992). Retrieval of aerosol optical properties from multi-angle satellite imagery. *IEEE Trans. Geosci. Rem. Sens.* **30**, 223-230.

Martonchik, J.V. and J.E. Conel (1994). Retrieval of surface reflectance and atmospheric properties using ASAS imagery. *Proceedings of the IGARSS'94 Symposium* (Pasadena, CA).

Martonchik, J.V. (1995). Atmospheric correction of vegetation index using multi-angle measurements. *Proceedings of the IGARSS'95 Symposium* (Firenze, Italy).

Martonchik, J.V. (1997). Determination of aerosol optical depth and land surface directional reflectances using multi-angle imagery. *J. Geophys. Res* **102**, 17,015-17,022.

Martonchik, J.V., D.J. Diner, R. A. Kahn, T.P. Ackerman, M. M. Verstraete, B. Pinty, and H.R. Gordon,(1998). Techniques for retrieval of aerosol properties over land and ocean using multiangle imagery. *IEEE Trans. Geosci. Rem. Sens.* **36,** 1212-1227

Minnis, P., P.W. Heck, and D.F. Young (1993). Inference of cirrus cloud properties using satellite-observed visible and Infrared radiances. Part II: Verification of theoretical cirrus radiative properties. *J. Atmos. Sci.* **50**, 1305-1322.

Mishchenko, M.I., and L.D. Travis (1994). Light scattering by polydisperse, rotationally

symmetric nonspherical particles: Linear polarization. *J. Quant. Spectrosc. Radiat. Transfer* **51**, 759-778.

Mishchenko, M.I., A.A. Lacis, B.E. Carlson, and L.D. Travis (1995). Nonsphericity of dust-like tropospheric aerosols: Implications for aerosol remote sensing and climate modeling, *Geophys. Res. Lett.* **22**, 1077-1080.

Mishchenko, M.I., L.D. Travis, R.A. Kahn, and R.A. West (1997). Modeling phase functions for dust-like tropospheric aerosols using a shape mixture of randomly oriented polydisperse spheroids. *J. Geophys. Res.* **102**, 16,831-16,847

Mishchenko, M. I., W. B. Rossow, A. Mache, and A. Lacis (1996). Sensitivity of cirrus cloud albedo, bidirectional reflectance, and optical thickness retrieval accuracy to ice particle shape. *J. Geophys. Res.* **101**, 16,973-16,985.

Myneni, R.B. and G. Asrar (1993). Radiative transfer in three-dimensional atmosphere-vegetation media. *J. Quant. Spectrosc. Radiat. Transfer* **49**, 585-598.

Nicodemus, F. E., J. C. Richmond, J. J. Hsia, I. W. Ginsberg, and T. Limperis (1977). *Geometrical Considerations and Nomenclature for Reflectance*, NBS Monograph **160**, National Bureau of Standards, U.S. Department of Commerce, Washington, D.C.

North, P.R.J., S.A. Briggs, S.E. Plummer, and J.J. Settle (1999). Retrieval of land surface bidirectional reflectance and aerosol opacity from ATSR-2 multiangle imagery. *IEEE Trans. Geosci. Rem. Sens.* **37**, 526-537

Pinty, B. and M. M. Verstraete (1992). GEMI: A non-linear index to monitor global vegetation from satellites. *Vegetatio* **101**, 15-20.

Preisendorfer, R.W. (1988). *Principal component analysis is meteorology and oceanography*. Elsevier, NY, 425 pp.

Rao, C. R. N., L. L. Stowe, and E. P. McClain (1989). Remote sensing of aerosols over the oceans using AVHRR data: Theory, practice and applications. *Int. J. Remote Sensing* **10**, 743-749.

Rahman, H., B.Pinty, and M.M. Verstraete (1993). Coupled Surface-Atmosphere Reflectance (CSAR) model. 2. Semiempirical surface model usable with NOAA Advanced Very High Resolution Radiometer data. *J. Geophys. Res*. **98**, 20,791-20,801.

Sassen, K., D. Starr, and T. Uttal (1989). Mesoscale and microscale structure of cirrus clouds: Three case studies. *J. Atmos. Sci.* **46**, 371-396.

Shettle, E.P., and R.W. Fenn, (1979). Models for the aerosols of the lower atmosphere and the effects of humidity variations on their optical properties. AFGL-TR-79-0214, Air Force

Geophysics Laboratory, pp. 94.

Stowe, L. L., R. M. Carey, and P. P. Pellegrino (1992). Monitoring the Mt. Pinatubo aerosol layer with NOAA/11 AVHRR data. *Geophys. Res. Lett.* **19**, 159-162.

Stowe, L.L., A.M. Ignatov, and R.R. Singh (1997). Development, validation, and potential enhancements to the second-generation operational aerosol product. J. Geophys. Res. **102**, 16,923-16,934.

Takano, Y., and K-N Liou (1989). Solar radiative transfer in cirrus clouds. Part I: Single-scattering properties of hexagonal ice crystals. *J. Atmos. Sci.* **46**, 3-19.

Verstraete, M. M., B. Pinty, and R.E. Dickinson (1990). A physical model of the bidirectional reflectance of vegetation canopies. 1. Theory. *J. Geophys. Res.* **95**, 11,775-11,765.

Wang, M. and H. R. Gordon (1994). Estimating aerosol optical properties over the oceans with MISR: Some preliminary studies. *Appl. Opt.* **33**, 4042-4057.

Williamson, S. J. (1972). *Fundamentals of Air Pollution.* Addison-Wesley, MA.

World Meteorological Organization ( WMO) (1988). Report of the International Ozone Trends Panel, Global Ozone Research and Monitoring Project -- Report No. 18.

World Climate Programme WCP-112 (1984). A Preliminary Cloudless Standard Atmosphere for Radiation Computation. IAMAP (International Association for Meteorology and Atmospheric Physics), Boulder, CO, pp.53.